THESIS SUMMARY

Iron is well known to be an important initiator of free radical oxidations, such as lipid peroxidation. However, the detailed mechanism for the initiation of lipid peroxidation is extremely complex. Many chemical species have been proposed to be able to serve as the initiators for these oxidations. At present, two iron-mediated mechanisms for initiating lipid peroxidation have received much attention.

- The favored mechanism, called the hydroxyl ($^{\bullet}$OH)-dependent mechanism, proposes that these oxidations are initiated by the hydroxyl radical;
- An alternate mechanism, hydroxyl-independent, proposes that iron-oxygen complexes rather than $^{\bullet}$OH radical initiates these oxidations.

In the first mechanism, iron serves either as a catalyst for the Haber-Weiss reaction or as a reagent for the Fenton reaction to form $^{\bullet}$OH, which eventually initiates lipid peroxidation. In the second mechanism, however, it has been proposed that lipid peroxidation is not initiated by $^{\bullet}$OH but rather by iron in the form of iron-oxygen complexes, such as perferryl ion or ferryl ion.

In this thesis, chemical (ethanol and dimethyl sulfoxide), biochemical (glucose, glyceraldehyde), and cellular (L1210 murine leukemia cells) targets were used to probe the abilities of these two mechanisms in initiating free radical oxidations. EPR spin trapping and oxygen monitor methods were used to compare the efficiency of Fe^{2+}-

initiated oxidations in the presence of H_2O_2 or O_2. To estimate how important are iron-oxygen complexes and $^{\bullet}OH$ radical in initiating biological free radical oxidations, the above methods were used with various experimental ratios of $[O_2]/[H_2O_2]$. The physiological ratio of $[O_2]/[H_2O_2]$ we estimate from reports to be about 100,000/1. When the experimental ratio $[O_2]/[H_2O_2] \geq 100/1$, our results suggest that the Fenton reaction plays a minor, perhaps insignificant role in initiating free radical oxidations; iron-oxygen complexes appear to dominate the initiation of free radical oxidations. Thus, we propose that the superoxide-driven Fenton reaction is probably a pathway for the initiation of some biological free radical oxidations, however, we suggest that iron-oxygen complexes are the primary route to the initiation of biological free radical oxidations.

CHAPTER I

INTRODUCTION

It is well known that the exposure of biological membranes to oxidizing species will induce progressive degeneration of membrane structure. Lipids containing unsaturated fatty acyl moieties are the common targets for oxidative attacks. This degradation process is generally termed lipid peroxidation. Lipid peroxidation may result in damage to a variety of organic components in living cells and is involved in several disease states [1-3], such as postischemic reperfusion injury, xenobiotic toxicity, and leucocyte-mediated inflammation. At present, there are at least two widely proposed mechanisms for the initiation of lipid peroxidation. The identification of possible initiators of lipid peroxidation is important to the understanding of the mechanisms of cell or tissue damage and to guide therapies against lipid peroxidation-induced pathologies.

In this introduction, the fundamentals of lipid peroxidation, iron's role in these oxidations, and two iron-mediated mechanisms for initiating oxidations are summarized. In addition, the goals and methods of this research are briefly presented.

Lipid Peroxidation — A Free Radical Process

Biological macromolecules, such as lipids, proteins, and DNA, are all targets for free radical injury [4]. Lipids, usually a polyunsaturated fatty acid moiety (PUFA), have

been extensively studied not only because of their function and structure but also because they are easily oxidized.

The lipid peroxidation process is a free radical event consisting of three distinct steps [5, 6]: initiation, propagation, and termination. The initiation step of lipid peroxidation can be expressed by reaction 1:

$$L\text{-}H + X^{\bullet} \rightarrow L^{\bullet} + XH \quad (1)$$

Where L-H represents the lipid, and $X^{\bullet}$ represents a highly oxidizing species such as hydroxyl radical or ferryl and perferryl species. In this reaction, a weakly bonded hydrogen atom is abstracted from L-H by $X^{\bullet}$, converting the lipid to a lipid radical ($L^{\bullet}$).

In the propagation phase of lipid peroxidation, $L^{\bullet}$ rapidly reacts with O_2 to form a lipid peroxyl radical ($LOO^{\bullet}$) (reaction 2). And then the $LOO^{\bullet}$ abstracts a hydrogen atom from another lipid to form a lipid hydroperoxide (LOOH) and a new $L^{\bullet}$ (reaction 3).

$$L^{\bullet} + O_2 \rightarrow LOO^{\bullet} \quad (2)$$

$$LOO^{\bullet} + L\text{-}H \rightarrow L^{\bullet} + LOOH \quad (3)$$

Reactions 2 and 3 comprise the propagation cycle of lipid peroxidation. See the box in Figure 1.

Termination of lipid peroxidation occurs when lipid radical species, produced during initiation or propagation, react with each other forming nonradical products, reactions 4-6:

$$2(LOO^{\bullet}) \rightarrow \text{nonradical products} \quad (4)$$

$$2(L^{\bullet}) \rightarrow \text{nonradical products} \quad (5)$$

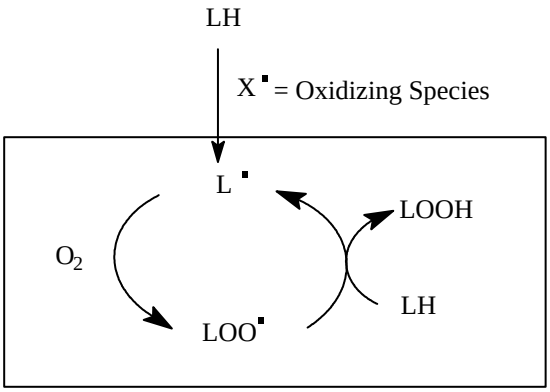

Figure 1. The scheme of lipid peroxidation. The box represents the propagation cycle of lipid peroxidation. If sufficient O_2 and lipid are available, this cycle will continue, resulting in the continuation of lipid peroxidation.

$$L^{\bullet} + LOO^{\bullet} \rightarrow \text{nonradical products} \quad (6)$$

Iron in Lipid Peroxidation

Iron plays a detrimental role in free radical-mediated oxidations, such as lipid peroxidation, by several mechanisms. In the initiation step, iron can serve as a catalyst for generating $^{\bullet}OH$ by the Haber-Weiss reaction, or it can directly initiate oxidations by forming iron-oxygen complexes, ferryl or perferryl ions. All of these species are highly oxidizing and are able to initiate free radical oxidations.

Iron also has another potential role in lipid peroxidation. In the propagation step, iron can react with LOOH in a reaction parallel to the Fenton reaction to form alkoxyl radicals ($LO^{\bullet}$) (reaction 7). The alkoxyl radical is usually believed to abstract a hydrogen atom from lipid chains, thereby initiating an additional radical chain and propagating lipid peroxidation, reaction 8 [6].

$$LOOH + Fe^{2+} \rightarrow LO^{\bullet} + OH^{-} + Fe^{3+} \quad (7)$$

$$LO^{\bullet} + L\text{-}H \rightarrow LOH + L^{\bullet} \quad (8)$$

However, due to its very short life times, the lipid alkoxyl radical might have too low steady state concentration to make a significant contribution in propagation of lipid peroxidation. Thus, Marnett and Wilcox [7] proposed another role for lipid alkoxyl radical for lipid propagation. According their mechanism (Figure 2), lipid alkoxyl radicals rapidly rearrange to form epoxyallylic radicals, which further react with oxygen yielding epoxyperoxyl radicals. The epoxyperoxyl radical may be responsible for most of

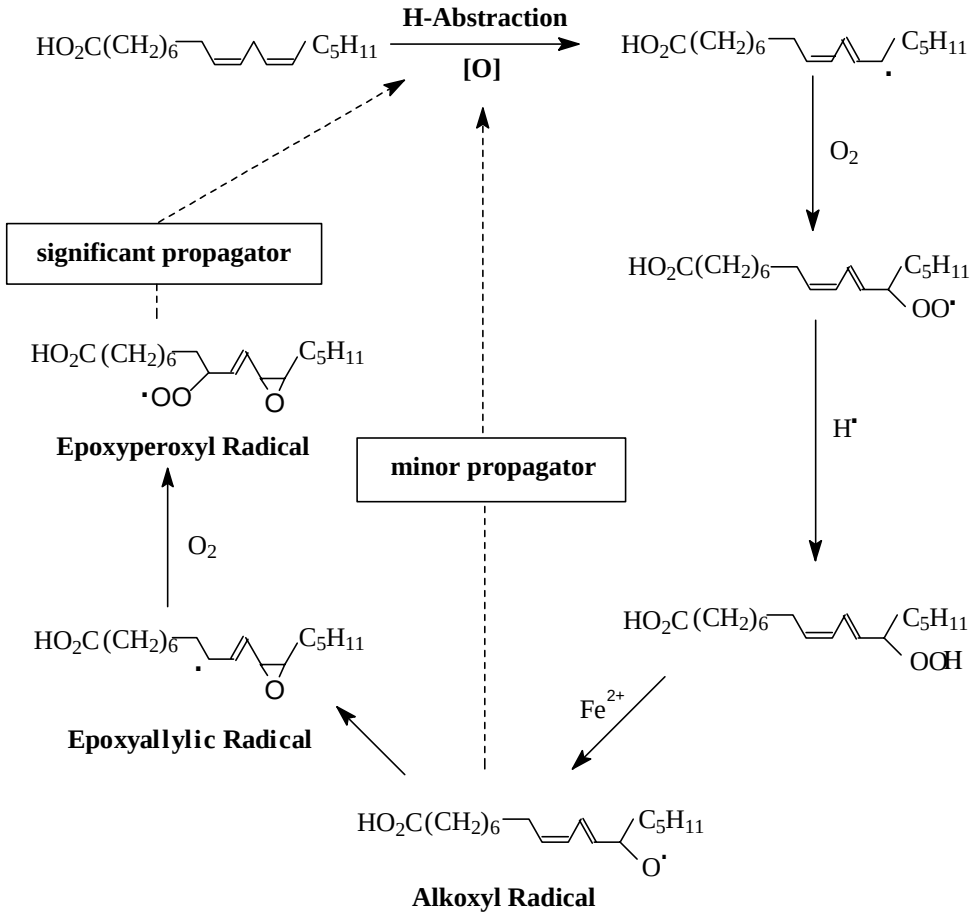

Figure 2. The role of alkoxyl radical in metal-mediated lipid peroxidation [7].

metal-propagated lipid peroxidation, *i.e.* it serves as an efficient propagator of lipid peroxidation.

The other type of reaction of alkoxyl radical is β-scission, which induces a chain-branching event (reaction 9).

$$LO^{\bullet} \rightarrow \text{Chain Branching by } \beta\text{-scission} \qquad (9)$$

For example, the reaction of Fe^{2+} with a hydroperoxide on the sixth carbon from the methyl end of a PUFA will produce pentane gas by β-scission, reactions 10-12.

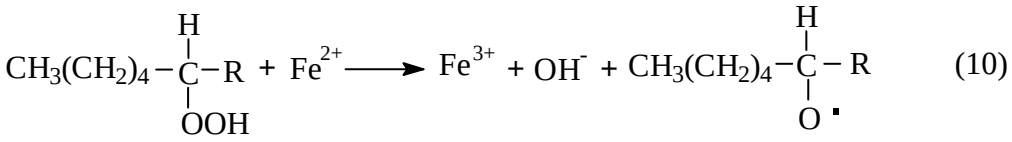

(10)

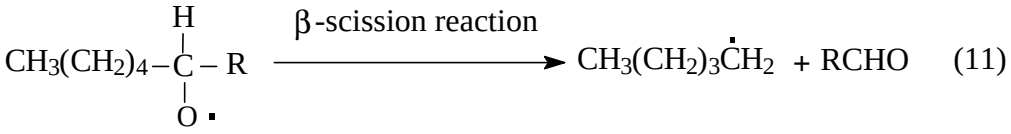

(11)

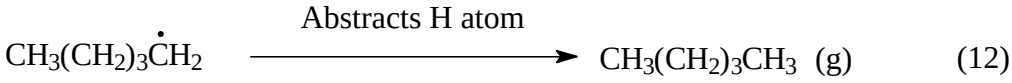

(12)

To clarify the role of iron in the initiation mechanism of lipid peroxidation is an important research problem because it will allow us to understand the mechanisms of cell and tissue injury, thereby allowing us to develop better therapies for these pathologies. Therefore, the principal goal of this research is to gain a better understanding of the role of iron in the initiation of free radical oxidations.

Iron-Mediated Mechanisms for Initiation Reactions

Iron has been proposed to initiate lipid peroxidation *via* two mechanisms: (i) by catalysis of •OH formation; or (ii) by reacting with oxygen to form oxidizing iron-oxygen complexes. The theoretical aspects and the experimental evidence of •OH involvement as well as lack of •OH involvement in initiating lipid peroxidation are presented in this section.

The •OH-Dependent Mechanism

The key step for lipid peroxidation is hydrogen atom abstraction from the fatty acid chain. Fatty acids can have three kinds of carbon-hydrogen bonds (Figure 3), each with different dissociation energies [6, 8]. The weakest of these three bonds is the carbon-hydrogen bond at the *bis*-allylic position with a dissociation energy of 75-80 kcal/mol. The dissociation energies for monoallylic carbon-hydrogen bonds and alkyl carbon-hydrogen bonds are 88 kcal/mol and 101 kcal/mol, respectively.

The hydroxyl radical is one of the most reactive oxidants that can be formed in a biological system. It is a highly reactive radical due to its structural characteristics. The lewis dot structure of •OH is shown in Figure 4. The four outermost orbitals of •OH have only seven electrons. Therefore, it has a great tendency to combine with one more electron to form the stable state — eight electrons in the outmost orbitals. To gain this eighth electron, it may abstract a hydrogen atom from a fatty acid chain, thereby initiating lipid peroxidation. Energetically, the ability of •OH to overcome the dissociation energy of carbon-hydrogen bond in fatty acid chains is unquestionable. The reaction of •OH

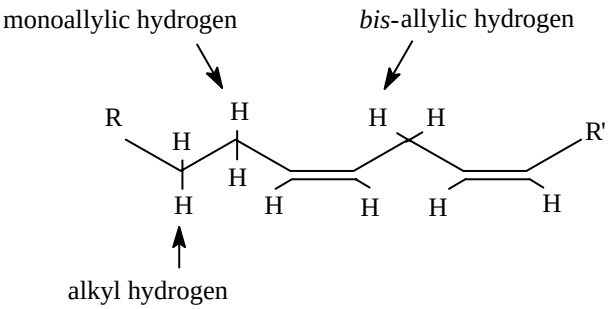

Figure 3. Fatty acid chain structure. The dissociation energies of different C-H bonds in fatty acid chain are 75-80 kcal/mol for *bis*-allylic, 88 kcal/mol for monoallylic, and about 101 kcal/mol for alkyl positions.

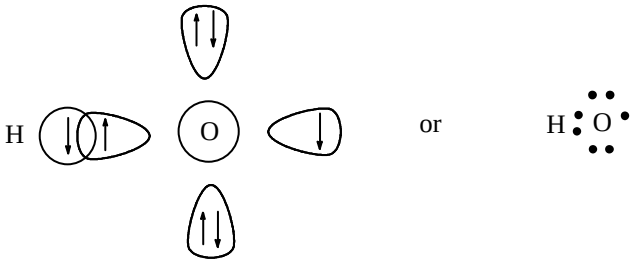

Figure 4. The lewis dot structure of •OH. Seven electrons in its outermost orbitals is the reason for hydroxyl radical being very reactive. It has a great tendency to get one more electron to form the stable state, *i.e.* eight electrons in the outmost orbitals.

combining with hydrogen atom is a exothermic reaction that releases about 119 kcal/mol of energy (reaction 13).

$$^{\bullet}OH + {}^{\bullet}H \rightarrow H_2O \qquad \Delta H = -119 \text{ kcal/mol} \qquad (13)$$

The energy required to dissociate a carbon-hydrogen bond on a lipid chain varies from 75-80 kcal/mol to 101 kcal/mol (reaction 14).

$$L\text{-}H \rightarrow L^{\bullet} + H^{\bullet} \qquad \begin{matrix} \Delta H = 75 \text{ kcal/mol } (\textit{bis}\text{-allylic C-H}) \\ \Delta H = 88 \text{ kcal/mol (monoallylic C-H)} \\ \Delta H = 101 \text{ kcal/mol (alkyl C-H)} \end{matrix} \qquad (14)$$

Thus, the net reaction, 13 + 14, *i.e.* the lipid peroxidation initiated by $X^{\bullet}$ (reaction 1, $X^{\bullet} = {}^{\bullet}OH$) is thermodynamically permitted. For example, ΔH for the net reaction of hydroxyl radical abstracting H atom from *bis*-allylic bond and forming H_2O is about -44 kcal/mol.

In the 1930's, F. Haber and J. J. Weiss proposed reaction 15 as an intermediate reaction for the decomposition of H_2O_2 [9]. This reaction has since become known as the Haber-Weiss reaction.

$$O_2^{\bullet -} + H_2O_2 \rightarrow O_2 + OH^- + {}^{\bullet}OH \qquad (15)$$

In the $^{\bullet}OH$-dependent mechanism for lipid peroxidation, the formation of $^{\bullet}OH$ was first thought to occur *via* the Haber-Weiss reaction. However, it is now known that this reaction proceeds at an insignificant rate, unless transition metals such as iron, copper, or perhaps cobalt are present [10, 11]. Therefore, a more logical expression of the Haber-Weiss reaction is:

$$Fe^{3+} + O_2^{\bullet-} \rightarrow O_2 + Fe^{2+} \quad (16)$$

$$2H^+ + 2O_2^{\bullet-} \rightarrow O_2 + H_2O_2 \quad (17)$$

$$Fe^{2+} + H_2O_2 \rightarrow OH^- + {}^{\bullet}OH + Fe^{3+} \quad (18)$$

Reaction 18 is the Fenton reaction. Thus, the Haber-Weiss reaction is more appropriately called the "superoxide-driven Fenton reaction" or "superoxide-dependent Fenton reaction".

The ${}^{\bullet}OH$-dependent initiation mechanism in lipid peroxidation has been demonstrated by several investigators. K. L. Fong *et al*. [12] reported that microsomes can catalyze the peroxidation of lysosomal membranes in the presence of ADP-Fe^{3+} and NADPH. They proposed a mechanism based on the formation of $O_2^{\bullet-}$ by cytochrome *P*-450 reductase (reaction 19), coupled with the superoxide-driven Fenton reaction as follows:

$$2O_2 + NADPH \xrightarrow{P\text{-}450} NADP^+ + H^+ + 2O_2^{\bullet-} \quad (19)$$

$$O_2^{\bullet-} + Fe^{3+} \rightarrow O_2 + Fe^{2+} \quad (16)$$

$$2O_2^{\bullet-} + 2H^+ \rightarrow O_2 + H_2O_2 \quad (17)$$

$$Fe^{2+} + H_2O_2 \rightarrow OH^- + {}^{\bullet}OH + Fe^{3+} \quad (18)$$

In agreement with this scheme, adding SOD (to remove $O_2^{\bullet-}$ for reducing Fe^{3+} to Fe^{2+} by reaction 16), catalase (to remove H_2O_2 for reaction 18), and ${}^{\bullet}OH$ scavengers (to intercept ${}^{\bullet}OH$ before it reacts with PUFA) all were reported to inhibit the peroxidation of lysosomal membranes.

Several years later, Lai *et al*. [13-15] presented evidence of $^{\bullet}OH$ involvement in the initiation of lipid peroxidation with almost the same experiment, except ADP-Fe^{3+} was replaced by EDTA-Fe^{2+}. Peroxidation was inhibited by catalase and $^{\bullet}OH$ traps, but stimulated by SOD according to the following scheme:

$$2O_2 + NADPH \xrightarrow{P\text{-}450} NADP^+ + H^+ + 2O_2^{\bullet-} \quad (19)$$

$$2O_2^{\bullet-} + 2H^+ \rightarrow O_2 + H_2O_2 \quad (17)$$

$$Fe^{2+} + H_2O_2 \rightarrow OH^- + {}^{\bullet}OH + Fe^{3+} \quad (18)$$

The evidence for $^{\bullet}OH$ involvement in the initiation of lipid peroxidation also has been provided by Girotti and Thomas [16, 17]. In their experiments, $O_2^{\bullet-}$ and H_2O_2 were generated by xanthine oxidase; free Fe^{3+} was present to catalyze the Haber-Weiss reaction.

However, many researchers [18] have found that lipid peroxidation is frequently insensitive to $^{\bullet}OH$ scavengers and SOD, and can even be enhanced by the addition of CAT. To explain these results, alternate ‘initiators’ iron-oxygen complexes such as ferryl and perferryl were proposed [19-22].

The $^{\bullet}OH$-Independent Mechanism

The theoretical and experimental aspects for supporting $^{\bullet}OH$-dependent initiation mechanism have been summarized. This part will focus on those aspects that actually argue against $^{\bullet}OH$ as an important initiator of lipid peroxidation.

As mentioned above, the ability of $^{\bullet}OH$ to behave as a powerful oxidant of

unsaturated lipids is unquestionable. However, the yield of $^{\bullet}OH$ in biological systems from the iron-catalyzed Haber-Weiss reaction will be extremely low because of the small rate constant of the Fenton reaction (reaction 18), only about 10^3 $M^{-1}s^{-1}$ [23] at physiological condition. Thus, the oxidation of Fe^{2+} by superoxide ($O_2^{\bullet-}$) (reaction 20) may have a significant role due to its much higher rate constant (about 10^7 $M^{-1}s^{-1}$) [24]. Kinetically, reaction 20 could completely overshadow the Fenton reaction (reaction 18), but it is frequently neglected.

$$Fe^{2+} + O_2^{\bullet-} \rightarrow H_2O_2 + Fe^{3+} \qquad (20)$$

It is also essential to realize that $^{\bullet}OH$ has a limited ability to diffuse. It is difficult to conceive that $^{\bullet}OH$ migrates from sites of generation to hydrophobic membrane compartments where lipid peroxidation is triggered without reacting with other biomolecules. For example, chelators existing in the body, such as ADP and citrate, are themselves rather good scavengers and could therefore intercept $^{\bullet}OH$ before it diffuses toward the lipid surface.

Perhaps the most important reason to consider iron-oxygen complexes rather than hydroxyl radical as initiators of biological oxidations is that the steady-state concentration of oxygen is much greater than hydrogen peroxide in living systems. In most regions of cells, $[H_2O_2]_{ss}$ for the Fenton reaction may be too low to have biological significance. For example, the steady-state red blood cell concentration of H_2O_2 is estimated to be approximately 10^{-10} M [25]. The hydroxyl radical formation rate can be expressed as:

$$\text{rate } (^{\bullet}OH \text{ formation}) \approx k_{Fenton} [H_2O_2]_{ss}[Fe^{2+}]$$

$$\approx (10^3\ M^{-1}s^{-1})(10^{-10}\ M)[Fe^{2+}]$$

$$\approx 10^{-7}\ s^{-1}[Fe^{2+}].$$

In vivo, however, $[O_2]_{ss}$ is about 10^{-5}-10^{-6} M [26] much higher than $[H_2O_2]_{ss}$ and could bind readily to $[Fe^{2+}]_{ss}$ forming Fe^{2+}-O_2 complexes. If we assume that the rate constant for oxidation of substrate by iron-oxygen complexes: $k_{Fe\text{-}O} \approx k_{Fenton}$ and that the oxidizable substrate concentration of a living system is about 1.5 M [*], the oxidation rate by iron oxygen complexes can be estimated below:

$$\text{rate (substrate oxidized)} \approx k_{Fe\text{-}O}[Fe^{2+}\text{-}O_2][\text{oxidizable substrate}]$$

$$\approx (10^3\ M^{-1}s^{-1})\ [Fe^{2+}\text{-}O_2]\ (1.5\ M)$$

$$\approx 1.5 \times 10^3[Fe^{2+}].$$

Thus, the rate of oxidation of oxidizable substrate by iron-oxygen complexes would be 10^{10} faster than the rate of oxidation by the Fenton reaction. Therefore, iron-oxygen complexes should dominate the initiation of biological free radical oxidations. The properties of two iron-oxygen complexes, *i.e.* perferryl and ferryl ions, are summarized below.

∗ In living systems the percentage by weight of oxidizable components (protein, lipid, and the bases of DNA) ≈ 30 %. From their average molecular weight: 110, 280, and 130 Da respectively, we estimate that the average oxidizable substrate molecular weight is ≈ 200 Da. Thus, the oxidizable substrate concentration is ≈ 300 g/1000 g ≈ (300 g/200 g mol^{-1})/L ≈ 1.5 M.

Perferryl ion

One of the iron-oxygen complexes is the perferryl ion. In an Fe^{2+}-aerobic solution, Fe^{3+} and $O_2^{\bullet-}$ are thought to be produced through the intermediate product, perferryl species, which is a structural intermediate between an Fe^{2+}-O_2 complex and an Fe^{3+}-$O_2^{\bullet-}$ complex. See reaction 21.

$$Fe^{2+} + O_2 \Leftrightarrow [Fe^{2+}\text{-}O_2 \Leftrightarrow Fe^{3+}\text{-}O_2^{\bullet-}] \Leftrightarrow Fe^{3+} + O_2^{\bullet-} \qquad (21)$$

Perferryl ion

Thus, the perferryl ion can be represented as a combination of Fe^{2+} with molecular oxygen (Fe^{2+}-O_2) and/or as the combination of Fe^{3+} with superoxide (Fe^{3+}-$O_2^{\bullet-}$). Another common representation of perferryl ion is Fe^{5+}=O. The formal charge of iron in perferryl ion (+5) as shown. Its high electron affinity is the reason that this species could replace $^{\bullet}OH$ as the ultimate oxidant for biological oxidations.

Evidence for perferryl ion-dependent lipid peroxidation has been provided by Aust and Svingen [22, 27], as well as Svingen and Tien [28, 29]. According to their observations, xanthine oxidase-dependent lipid peroxidation and NADPH-dependent lipid peroxidation are both mediated by perferryl ion. In the xanthine oxidase-mediated system, they found that the formation of Fe^{3+}-$O_2^{\bullet-}$ is inhibited by SOD, thereby resulting in inhibition of lipid peroxidation. In contrast, in an NADPH-dependent system, the formation Fe^{2+}-O_2 is not inhibited by SOD, and therefore SOD fails to inhibit peroxidation.

Ferryl ion

Another iron-oxygen complex that has received attention is ferryl ion. Its chemical representation can be Fe^{4+}=O, Fe^{2+}-O, or Fe^{4+}-O^{2-}. The formal charge of iron in ferryl ion is +4.

Ferryl ion is thought to be formed by two different mechanisms. The first relies on $O_2^{\bullet-}$-dependent reduction of Fe^{3+} to Fe^{2+} and subsequent reaction of Fe^{2+} with H_2O_2. Under proper conditions of pH and polarity, Fenton reagents will produce ferryl ion rather than $^{\bullet}OH$ [30]:

$$Fe^{3+} + O_2^{\bullet-} \rightarrow O_2 + Fe^{2+} \quad (22)$$

$$Fe^{2+} + H_2O_2 \rightarrow Fe^{2+}O + H_2O \quad (23)$$

The second mechanism for ferryl ion formation is by the reaction of perferryl ion with Fe^{2+}, according to the reactions 24 and 25 [27].

$$Fe^{2+} + Fe^{2+}\text{-}O_2 \rightarrow Fe^{2+}\text{-}O_2\text{-}Fe^{2+} \quad (24)$$

Perferryl ion

$$Fe^{2+}\text{-}O_2\text{-}Fe^{2+} \rightarrow 2Fe^{2+}\text{-}O \quad (25)$$

Ferryl ion

The possibility of ferryl ion initiating lipid peroxidation was investigated by Koppenol [31]. He found that NADPH-dependent Fe^{3+} reduction is accompanied by the simultaneous formation of both perferryl and ferryl ion, but xanthine oxidase-dependent lipid peroxidation is enhanced by CAT. These findings suggest that the availability of H_2O_2 for initiation of lipid peroxidation is not essential.

In our research, we used EPR spin trapping to compare the efficiency of the Fenton reaction *vs.* iron-oxygen complexes in initiating chemical, biochemical, and cellular free radical oxidations. We find that pre-existing H_2O_2 is not necessary for initiating free radical oxidations, *i.e*. all the oxidations can be initiated by Fe^{2+} in aerobic solution. Furthermore, in H_2O_2-free solutions, achieved by adding CAT, Fe^{2+} still can initiate free radical formation. Thus, we propose that iron-oxygen complexes are the primary initiators of free radical oxidations in biological systems.

Physiological Iron

Iron is essential for many life processes such as oxygen transport, electron transfer, nitrogen fixation, and DNA synthesis. Physiologically, iron is stored in ferritin, a ubiquitous protein containing a shell with a molecular weight about 450,000 Da and 24 subunits [32]. The ferritin shell can hold up to ≈ 4500 iron atoms. The low solubility of iron (10^{-18} M) at physiological pH is one of the reasons that chelators are present in living systems. Therefore, coordinated, *i.e*. chelated iron is the logical form that should be studied physiologically.

By definition, a chelator is a polydentate ligand in which two or more donor atoms, usually N, O, or S, are so arranged that they can coordinate to the same central metal, such as iron or copper. Nearly every biological molecule has N, O, or S to coordinate iron. For example, reduced flavins, cysteine, glutathione, all have chelation functions and can stimulate iron transport, *i.e*. release iron from ferritin to other living components.

In vitro studies indicate that chelation of iron can alter its redox potential, making its autoxidation (reaction 26) either more or less favorable [33].

$$Fe^{2+} + O_2 \rightarrow Fe^{3+} + O_2^{\bullet-} \quad (26)$$

Common chelators used in biochemical investigations are EDTA and DTPA. Both have a similar structure, except that Fe^{3+}-EDTA has a water coordination whereas Fe^{3+}- DPTA does not [34]. They are both able to enhance Fe^{2+}-chelator autoxidation (reaction 26), but DTPA greatly reduces the catalytic activity of iron for the Haber-Weiss reaction and EDTA slightly enhances the iron-catalyzed Haber-Weiss reaction by inhibiting (DTPA) or stimulating (EDTA) the reduction of Fe^{3+} by $O_2^{\bullet-}$ (reaction 27).

$$Fe^{3+}\text{-chelator} + O_2^{\bullet-} \rightarrow O_2 + Fe^{2+}\text{-chelator} \quad (27)$$

Figure 5 shows the chemical representation of EDTA and DTPA ions. The effects of EDTA and DPTA upon the Fenton reaction-mediated and iron-oxygen complex-mediated oxidations were investigated in this work.

Research Summary

The hypothesis of this research is that the Fenton reaction mechanism is a minor initiator of biological oxidations compared to the iron-oxygen complex mechanism. The points supporting this hypothesis are: 1) the low rate constant of the Fenton reaction; 2) the low H_2O_2 concentration present in cells and tissues; and 3) the much higher O_2 concentration compared to H_2O_2 concentration present at physiological conditions.

Based on literature reports [25, 26], we estimate that the physiological $[O_2]/[H_2O_2]$ is about 10^5. This ratio provides the kinetic basis for our hypothesis in that

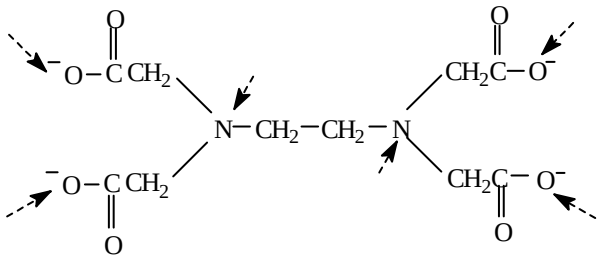

EDTA anion

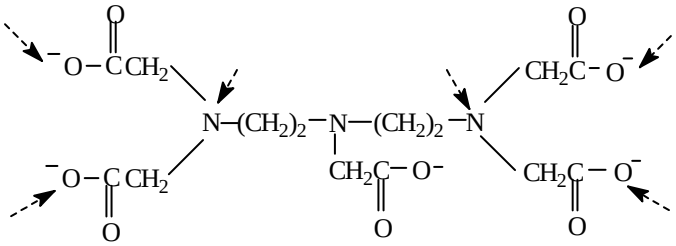

DTPA anion

Figure 5. The structures of EDTA and DTPA. The marked atoms coordinate with iron to form hexadentate chelation iron complex.

the oxidation rate due to iron-oxygen complexes might be much higher than the oxidation rate due to hydroxyl radical, which is formed by the Fenton reaction.

The oxidation targets used in our research include chemical (DMSO, EtOH), biochemical (glucose, glyceraldehyde), and tissue culture cells (lipid-modified L1210). Free radical formation by these oxidation targets was measured by EPR spin trapping with POBN. Oxygen monitor, the other method in our research, was used to measure the H_2O_2 that remained after the Fenton reaction. The interesting finding in our research is that free radical oxidations can be initiated by Fe^{2+} and/or Fe^{2+}-CAT. This suggests that (pre)-existing H_2O_2 is not necessary to initiate free radical oxidations. In other words, Fe^{2+} and O_2 may be the only reagents necessary for initiating free radical oxidations.

To examine this proposal, we compared radical yields from the Fenton reaction *vs.* radical yields from iron-oxygen complex reactions, *i.e.* we compared the Fenton reaction efficiency *vs.* iron-oxygen complex reaction efficiency in initiating oxidation of the targets under various experimental $[O_2]/[H_2O_2]$. With this information, we can then infer how important is the Fenton reaction in initiating free radical oxidations in living systems where very high $[O_2]/[H_2O_2]$ exists.

The results from the chemical and biochemical free radical oxidations suggest that the Fenton reaction efficiency significantly decreases as $[O_2]/[H_2O_2]$ increases. However, the cellular oxidation results show that H_2O_2 does not enhance free radical oxidation, but rather inhibits cellular radical formation. We conclude that, under physiological conditions, the Fenton reaction plays a minor role in initiating oxidation and that iron-oxygen complexes are the primary initiators of biological free radical oxidations.

CHAPTER II

MATERIALS AND METHODS

Materials

Phosphate Buffer Solutions

All experiments were performed in 50 mM (pH 7.4) potassium phosphate-buffered aqueous solution. The potassium dihydrogen phosphate (KH_2PO_4) and dipotassium hydrogen phosphate (K_2HPO_4) were purchased from Fisher.

The metal impurities existing in phosphate buffer were removed by treatment with chelating resin (sodium form, dry mesh 50-100) from Sigma. After washing the resin with portions of phosphate buffer several times to neutralize its strongly acidic or basic properties, the resin was then added to the phosphate buffer solution using about 10 ml of resin per liter of solution and very gently stirred for at least 12 hours. A pH value (7.4) for phosphate buffer was obtained adding HCl or NaOH (1M, Fisher) as necessary. This phosphate buffer solution was used after the resin was allowed to settle and after passing the ascorbate test.

The Ascorbic Test [35]

Ascorbic acid is a diacid, with pK_a values of 4.2 and 11.6. The spontaneous oxidation of ascorbate monoanion at pH 7.4 is very slow in the absence the catalytic metals, such as iron and copper. Thus, this catalytic ability can be used to test whether or not contaminating catalytic iron or copper are present in the phosphate buffer solution.

Ascorbic acid, purchased from Sigma, was prepared fresh as a 0.10 M stock solution with redistilled water resulting in a pH 2 colorless solution. To perform the ascorbic test, about 3.75 μl this ascorbate solution was mixed with 3.0 ml phosphate buffer solution. A Milton Roy Spectronic 3000 Array UV spectrophotometer was used to measure the absorbance at 265 nm. The initial absorbance at 265 nm ≈ 1.8. If adventitious metals are absent in the test solution, the absorbance should decrease by less 0.5% in 15 min.

POBN Spin Trap

The spin trap POBN, α-(4-pyridyl-1-oxide)-*N*-*tert*-butylnitrone, was purchased from Oklahoma Medical Research Foundation Spin Trap Source, Oklahoma city. POBN (1.0 M) was prepared as an aqueous stock solution before use in the oxidation systems. This stock solution was kept on ice during the experiment.

Fe^{2+} Solution

Ferrous ammonium sulfate ($Fe(NH_4)_2(SO_4)_2 \cdot 6H_2O$) was from Fisher Scientific Co. 10 mM stock solution of Fe^{2+} was prepared in redistilled water. The pH of the Fe^{2+} stock solution was controlled by HCl to keep it about 2.5. At this pH, Fe^{2+} is very stable.

H_2O_2 Solution

H_2O_2 (30%) was purchased from EM Science. A 10 mM stock solution was prepared with redistilled water. This concentration was verified using a Milton Roy Spectronic 3000 Array UV spectrophotometer to measure the absorbance at 240 nm ($\in_{240}$ = 44 M^{-1} cm^{-1}).

DMSO and EtOH

DMSO (Sigma) and 100% EtOH (Fisher) were directly introduced into the oxidation systems as needed to make 100 mM solutions. About 3 μL DMSO and 3.5 μL EtOH neat solutions were required to prepare 500 μl EPR samples.

Glucose

Glucose, purchased from EM Science, was prepared as 2.00 M stock solution with phosphate buffer immediately before introducing it into the oxidation system to make a 200 mM solution.

Chelators

EDTA and DTPA, purchased from Sigma, were dissolved in redistilled water by moderate heating to make 11.0 mM stock solutions. When chelated-Fe^{2+} solution was used, the ratio of EDTA or DTPA/Fe^{2+} were 1.1/1. N_2 or argon gas was used to remove oxygen keeping iron in the Fe^{2+} form, *i.e.* protect iron from autoxidation process before inducing chelated iron into the oxidation system.

SOD, CAT, and BSA

CAT (Sigma) and SOD (from Bovine Erythrocytes, Sigma) were prepared with redistilled water and then introduced into oxidation systems to make final concentration of 500 U/mL for CAT and 50 U/mL for SOD. Protein controls were performed using

BSA (Sigma) at the same protein concentration as in the SOD and CAT experiments.

L1210 Cells

L1210 murine leukemia cells were grown in a humidified atmosphere of 95% air-5% CO_2 at 37°C in RPMI 1640 (Grand Island Biochemical Co.) medium containing 10% fetal bovine serum (Sigma).

The cells were maintained as an exponentially growing culture by passage every 3 days. Cell lipids were modified by addition of 32 μM fatty acid DHA (Nu Chek Prep, MN) to the growth medium for 2 days. Before the EPR spin trapping experiment, the cells were washed three times with chelated phosphate buffer solution to remove any remaining fatty acid-supplemented growth medium. Cells were resuspended in the phosphate buffer solution at a density of 5×10^6 cells/mL for the EPR measurements.

The Order of Addition

The order of addition of reaction reagents is an important factor that may affect the results. In our experiments, the target materials were usually mixed with phosphate buffer before introducing any other reagents. The spin trap POBN and then H_2O_2 were added to the system. The Fe^{2+} solution was always added to the oxidation system last.

EPR and Spin Trapping

EPR is considered to be the only method we can use for directly observing free radicals. However, direct detection of the free radicals formed in complex biological systems is not always possible with the EPR method. The free radicals formed are

usually very reactive and have short lifetimes. These properties result in a very low steady state radical concentration, below the limit of EPR detection.

Spin trapping, a technique developed in the 1970's [36, 37], is considered to be a powerful tool to visualize biological free radicals indirectly. In this technique, a diamagnetic compound, called a spin trap, reacts with a primary free radical to form a more stable radical that can accumulate to a high enough concentration for study by EPR.

There are two categories of compounds that are commonly utilized as spin traps: nitrone and nitroso compounds. MNP, a popular nitroso compound, reacts with unstable radicals at its nitrogen position. See reaction 28.

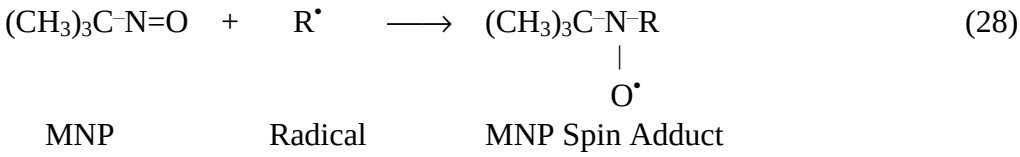

(28)

The advantage of MNP spin adduct is that it can yield a lot of structural information about the primary radical. With the MNP spin adducts, different primary radicals have different β-Hs, which will have different hyperfine splitting parameters.

However, oxygen-centered radicals reacting with MNP produce very unstable adducts that cannot be easily detected by EPR. Thus, nitrones are the common spin traps used for the study of biological free radical reactions. Reaction 29 represents the nitrone reaction with free radicals.

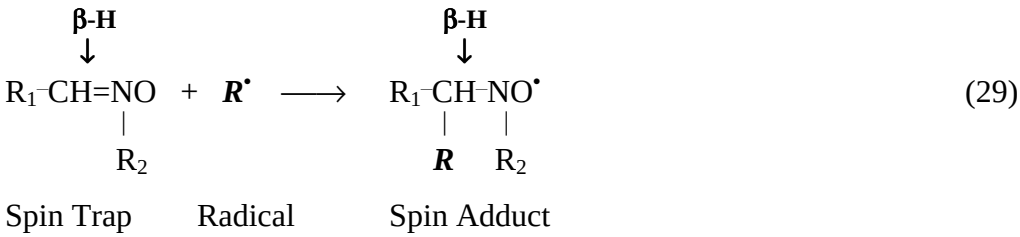

(29)

The structural information we can get from nitrone compounds will be less than that from nitroso compounds because the β-H is not from the trapped radical but from the nitrone compound. However, the most popular nitrone compounds, such as DMPO and POBN still can provide information from the hyperfine splitting parameters [38].

Most of the EPR spin trapping experiments in our work were performed using POBN as the spin trap. The chemistry of POBN reacting with the oxidative targets and EPR spectra of POBN spin adduct are presented below.

POBN Spin Trap and POBN Spin Adducts

POBN, α(4-pyridyl-1-oxide)-N-*tert*-butyl nitrone, was developed in 1978 [39]. It has been particularly useful in studying biological systems due to its good water solubility.

The free radicals formed from our target oxidations all are very unstable and have very short life-times. For example, the life time of $^{\bullet}CH_3$ is about 10^{-6} s. Thus, direct detection of these radicals *via* EPR is difficult, but is made much easier when a spin trap, such as POBN, is used. These unstable radicals ($R^{\bullet}$ in reaction 30) react with POBN to form a POBN spin adduct, a stable radical that can easily be observed by EPR.

POBN Spin Trapping During DMSO Oxidation

In DMSO oxidation, $R^{\bullet}$ represents radicals such as $^{\bullet}CH_3$ and $^{\bullet}OCH_3$. POBN reacts with these radicals to yield spin adducts as follows.

A. DMSO reacts with hydroxyl radical or iron-oxygen complexes to form methyl radical (reaction 31).

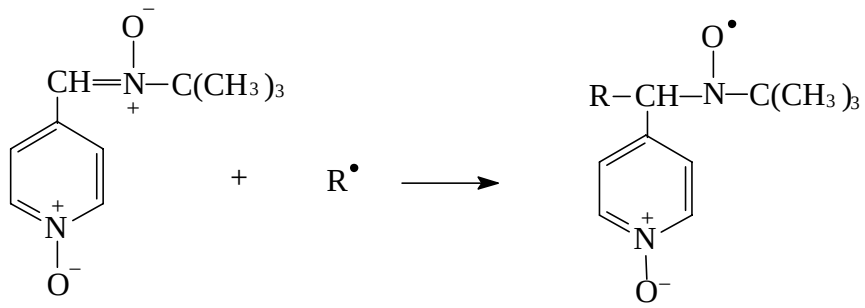

(30)

POBN Spin Trap Radical POBN spin adduct

$$DMSO + \text{oxidizing species} \longrightarrow {}^{\bullet}CH_3 + CH_3S(O)OH \quad (31)$$

($HO^{\bullet}$ or Perferryl/Ferryl ions)

B. Methyl radical can react with POBN to yield a EPR detectable spin adduct (reaction 32). Methyl radical can also react with O_2 to form a methyl peroxyl radical, which then decomposes to an alkoxyl radical *via* reactions 33 and 34.

$$^{\bullet}CH_3 + POBN \longrightarrow \underset{\text{EPR Detectable}}{POBN/^{\bullet}CH_3} \quad (32)$$

$$^{\bullet}CH_3 + O_2 \rightarrow {}^{\bullet}OOCH_3 \xrightarrow{H^{\bullet}} CH_3OOH \xrightarrow{Fe^{2+}} {}^{\bullet}OCH_3 \quad (33)$$

$$2\,{}^{\bullet}OOCH_3 \longrightarrow 2\,{}^{\bullet}OCH_3 + O_2 \quad (34)$$

C. The alkoxyl radical further reacts with POBN to produce another EPR detectable spin adduct. See reaction 35.

$$^{\bullet}OCH_3 + POBN \rightarrow \underset{\text{EPR Detectable}}{POBN/^{\bullet}OCH_3} \quad (35)$$

The ${}^{\bullet}OOCH_3$, formed from reaction 33, also can be trapped by POBN. But this spin adduct has a very short lifetime and therefore is not detectable in our experiments.

POBN Spin Trapping During EtOH Oxidation

In EtOH oxidation, the primary radical $R^{\bullet}$ represents the α-hydroxyethyl radical formed from EtOH reacting with hydroxyl radical or iron-oxygen complexes (reaction 36).

$$CH_3CH_2OH + \text{oxidizing species} \longrightarrow CH_3^{\bullet}CHOH + H_2O \quad (36)$$

($HO^{\bullet}$ or Perferryl/Ferryl ions)

α-Hydroxyethyl radical reacts with POBN to form a spin adduct that can be detected by EPR. See reaction 37.

$$CH_3^{\bullet}CHOH + POBN \longrightarrow POBN/\ CH_3^{\bullet}CHOH \quad (37)$$

EPR Detectable

POBN Spin Trapping During Glucose Oxidation

In glucose oxidation, the oxidizing species, *i.e*. hydroxyl radical or iron-oxygen complexes, may abstract a H atom from weak C-H bonds in glucose to form a glucose radical. The glucose radical can further react with POBN forming an EPR detectable spin adduct. This process can be represented by the following reactions.

$$\text{Glucose} + \text{oxidizing species} \longrightarrow {}^{\bullet}\text{Glucose} + H_2O \quad (38)$$

($HO^{\bullet}$ or Perferryl/Ferryl ions)

$${}^{\bullet}\text{Glucose} + POBN \longrightarrow POBN/{}^{\bullet}\text{Glucose} \quad (39)$$

EPR Detectable

POBN Spin Trapping During Cellular Oxidation

In our experimental conditions, the lipid fatty acid chains of cell membranes and lipoproteins are free radical oxidation targets. It is known that iron or other catalytic metals are usually required to initiate lipid peroxidation. However, it is in conflict with

the requirement of H_2O_2 to induce lipid peroxidation. Thus, the possible expression of the lipid-derived carbon-centered radical formation could be represented by reaction 40.

$$\text{Cellular lipid} + \text{Perferryl or Ferryl ions} \longrightarrow {}^{\bullet}\text{lipid} + H_2O \quad (40)$$
$$(\ ?\ HO^{\bullet})$$

The lipid-derived radicals can be detected by EPR spin trapping with POBN.

$${}^{\bullet}\text{Lipid} + \text{POBN} \longrightarrow \text{POBN}/{}^{\bullet}\text{Lipid} \quad (41)$$
$$\text{EPR Detectable}$$

EPR Measurements

All EPR spectra in our work were obtained with a Bruker ESP-300 spectrometer operating at 9.76 GHz and room temperature. The EPR spectrometer settings were: modulation frequency 100 kHz; modulation amplitude 1.0 G; microwave power 40 mW; receiver gain 10^5-10^6.

Desired reaction mixtures (500 μL for aerobic condition; 3 mL for anaerobic condition) were prepared in glass tubes by mixing phosphate buffer solution, oxidation target molecule, POBN, H_2O_2, and Fe^{2+} or chelated-Fe^{2+} in that order. The samples were then transferred to the EPR quartz flat cell and centered in a TM_{110} cavity.

Usually, a carbon centered-radical spin trapped with POBN shows a primary triplet splitting due to one of the N nuclei in POBN and secondary doublet splitting due to the β-hydrogen in POBN. Their different splitting constants result in EPR spectra having six hyperfine lines with the same intensity. For example, an EPR spectra with the splitting constant of N ($a^N \approx 15.8$ G) and the splitting constant of β-H ($a^H \approx 2.7$ G) will be detected in EtOH oxidation (Figure 6-a). However, EPR spectra will be more complex if

more than one radical are trapped by POBN. For example, two POBN spin adducts were detected by EPR from DMSO aerobic Fenton reaction (Figure 6-b).

Oxygen Monitor

The YSI model 53 Biological Oxygen Monitor is a polarographic system for measuring oxygen uptake or evolution. In our work, it was used to measure the oxygen yield from H_2O_2 reacting with CAT and therefore to estimate how much H_2O_2 remained after the Fenton reaction. Thus, this method provides stoichiometry information on the Fenton reagents during the free radical oxidations.

The heart of this system is the oxygen probe. It is a specially designed polarographic system consisting of a platinum cathode, silver anode, and KCl solution held captive around the electrodes by a membrane. Gases can penetrate through this membrane to enter the interior probe. When a suitable polarizing voltage is applied across the probe, oxygen will be consumed at the cathode causing a current to flow through the probe. The reaction on the probe is:

$$O_2 + 2H_2O + 4e^- \longrightarrow 4\ OH^- \qquad (42)$$

Thus, the amount of current is proportional to the amount of oxygen to which the membrane is exposed.

The probe actually measures the oxygen pressure. Since oxygen is rapidly consumed at the cathode, the oxygen pressure in the probe is near zero. The force

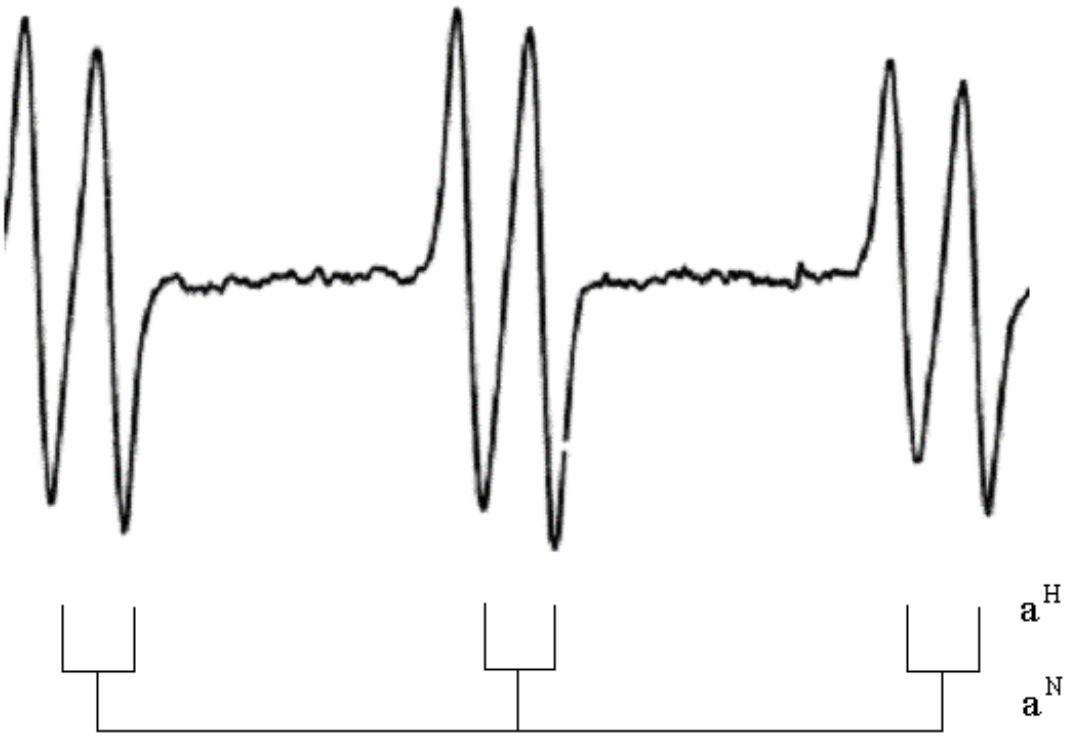

Figure 6. EPR spectra of POBN spin adduct.
(a) EPR spectrum of POBN spin adduct formed in EtOH oxidation. The hyperfine splitting constants are $a^N \approx 15.8$ G and $a^H \approx 2.7$ G. Spin adduct yield was measured by peak height or peak area of the central doublet.

Figure 6-continued

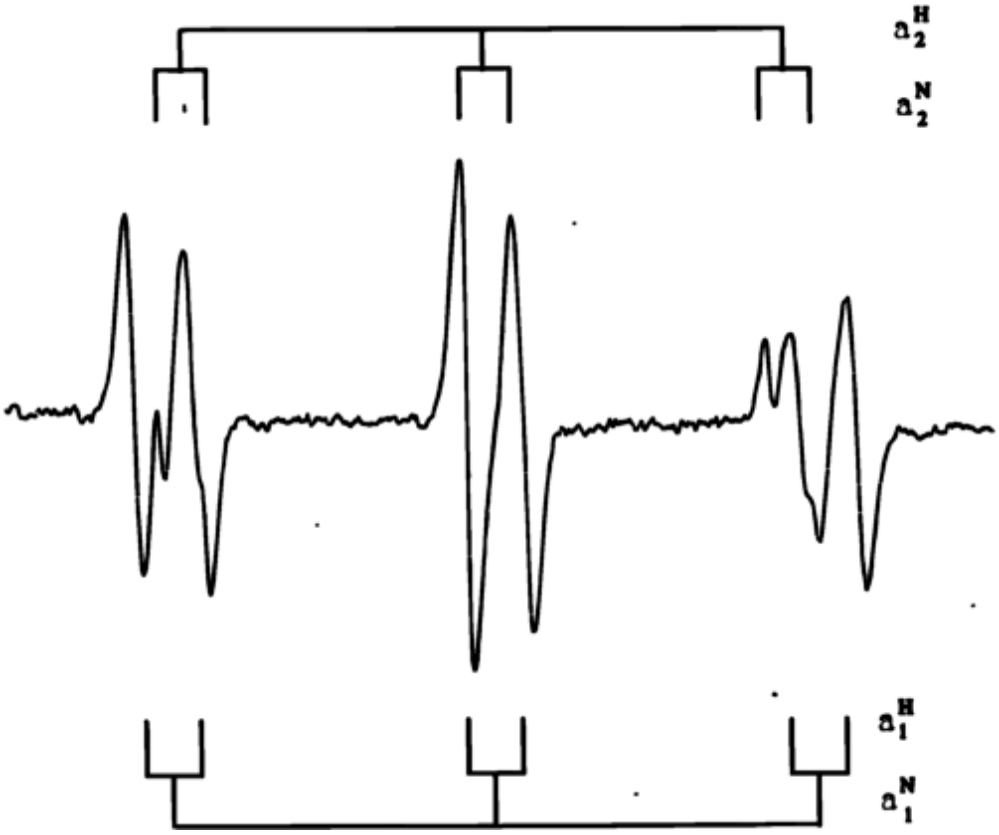

Figure 6. EPR spectra of POBN spin adduct.
(b) EPR spectrum of POBN adducts formed in DMSO oxidation under aerobic condition. The splitting constants of two adducts are: $a_1^N \approx 16.1$ G and $a_1^H \approx 2.8$ G; $a_2^N \approx 14.8$ G and $a_2^H \approx 2.4$ G. Total spin adduct yield was measured by peak height or peak area of the central doublet.

causing oxygen to diffuse through the membrane is proportional to the absolute pressure of oxygen outside the membrane. If oxygen pressure increases, more oxygen diffuses through the membrane and more current flows through the probe. However, a lower pressure results in less current. Thus, we can easily quantify H_2O_2 remaining in the system by measuring oxygen, which is derived from H_2O_2 by addition of CAT. See reaction 43.

$$2\,H_2O_2 \xrightarrow{\text{CAT}} O_2 + 2H_2O \qquad (43)$$

Therefore, we obtain H_2O_2 stoichiometry information for the Fenton reaction-mediated chemical oxidations by using the oxygen monitor method.

CHAPTER III

CHEMICAL FREE RADICAL OXIDATIONS

Results and Discussion

For chemical free radical oxidations DMSO and EtOH were chosen as oxidation targets in our research. DMSO and EtOH can rapidly react with oxidizing species, such as $^{\bullet}OH$. Thus, they are commonly used in biological free radical reactions as $^{\bullet}OH$ scavengers. One reason for DMSO and EtOH being chosen as the oxidation targets in our research is that the chemistry of DMSO and EtOH free radical oxidation is very well understood. The other is that the energies to decompose DMSO and EtOH during their oxidation are very close to the C-H bond dissociation energy in biological materials.

The goal for studying these chemical oxidations is to establish the experimental model to be used to address the research question — How important is the Fenton reaction or iron-oxygen complex reactions in initiating biological free radical oxidations ?

EPR spin trapping with POBN was used to measure free radical production from DMSO and EtOH oxidations that were initiated *via*: 1) the anaerobic Fenton reaction; 2) aerobic Fenton reaction; and 3) aerobic Fe^{2+} solution and/or Fe^{2+}-CAT solution. An oxygen monitor was used to measure how much H_2O_2 remained after the aerobic Fenton reaction. The EPR method was also used to study the effect of chelators, such as EDTA

and DTPA, on the Fenton reaction-mediated oxidation and iron-oxygen complex-mediated oxidation.

POBN Spin Adducts are Formed *via* the Authentic Fenton Reaction

There are two iron-mediated mechanisms considered to be capable of initiating free radical oxidations. They are the Fenton reaction and iron-oxygen complex mechanisms. The reagents required for the Fenton reaction are Fe^{2+} and H_2O_2, while the reagents for iron-oxygen complexes are Fe^{2+} and O_2 or Fe^{3+} and $O_2^{\bullet-}$. Thus, when chemical targets are exposed to H_2O_2 and Fe^{2+} under anaerobic conditions, the Fenton reaction should be considered as a pure Fenton reaction. Therefore, to examine this Fenton reaction kinetics we firstly studied EtOH and DMSO; their oxidations were initiated *via* the Fenton reaction under anaerobic conditions.

According to the chemistry of the reaction of DMSO or EtOH with $^{\bullet}OH$, a carbon-centered radical will be initially produced. It is the methyl radical ($^{\bullet}CH_3$) for DMSO (reaction 44), and α-hydroxyethyl radical $CH_3{}^{\bullet}CHOH$ for EtOH (reaction 45).

$$DMSO + {}^{\bullet}OH \longrightarrow {}^{\bullet}CH_3 + CH_3S(O)OH \quad (44)$$

$$CH_3CH_2OH + {}^{\bullet}OH \longrightarrow CH_3{}^{\bullet}CHOH + H_2O \quad (45)$$

These two radicals can not be directly observed by EPR under our experimental conditions due to their short lifetimes. However, the spin trap POBN can react with them to form EPR detectable spin adducts. See reactions 32 and 37.

EPR spectra of POBN/$^{\bullet}CH_3$ is very similar to the spectra of POBN/$CH_3{}^{\bullet}CHOH$ (see Figure 6-a). The hyperfine splitting constants from N atom (represented as a^N) of

these adducts have values: 16.1 G for POBN/$^{\bullet}CH_3$ and 15.8 G for POBN/$CH_3{}^{\bullet}CHOH$. But the splitting constants of the β-H in both spin adducts are nearly identical, ≈ 2.7-2.8 G.

Under anaerobic conditions, POBN spin adduct yield *vs*. [Fe^{2+}] in DMSO/EtOH Fenton oxidation is shown in Figure 7. In these experiments, EPR samples contained 100 mM DMSO or EtOH; 10 mM POBN; 200 μM H_2O_2; and various [Fe^{2+}] (0, 12.5, 25, 50, and 100 μM). As shown in Figure 7, the yield of spin adducts has an iron-dependent relationship that suggests 1:1 stoichiometry for Fe^{2+} to form spin adduct for most [Fe^{2+}] conditions. Only at high [Fe^{2+}] ≈ 100 μM, did the production of POBN spin adducts not fit the 1:1 relationship well. Fe^{2+} addition under high [Fe^{2+}] did not further enhance radical formation as well as anticipated from the data at low [Fe^{2+}]. A possible interpretation is that at high [Fe^{2+}], ferrous will also undergo reaction 46 to scavenge hydroxyl radical, and thereby inhibit oxidative target-radical formation.

$$Fe^{2+} + {}^{\bullet}OH \longrightarrow Fe^{3+} + OH^{-} \qquad (46)$$

To our surprise, EPR studies of various [H_2O_2] with excess [Fe^{2+}] under anaerobic conditions did not provide H_2O_2 stochiometric information well. When excess [Fe^{2+}] is used, the yield of POBN spin adduct is very low, close to the control experiment in which 0 μM Fe^{2+} was used (see Figure 8). The possible reason for this is that Fe^{2+} might destroy the POBN spin adduct under anaerobic conditions.

This stochiometric information will be used to compare the stoichiometry of other oxidation models, *i.e.* aerobic Fenton reaction or iron-oxygen complex reaction models,

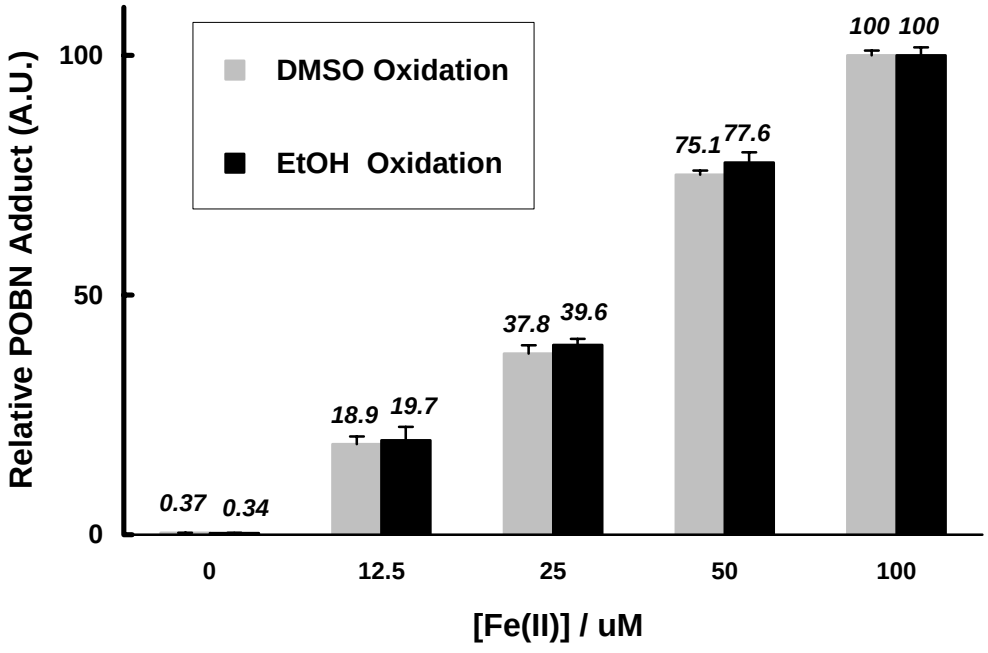

Figure 7. POBN adduct yield *vs*. [Fe^{2+}] in chemical oxidations that are mediated by the anaerobic Fenton reaction. 100 mM DMSO or EtOH oxidized by 200 μM H_2O_2 and 0-100 μM Fe^{2+}. The ordinate represents the POBN adduct yield in arbitrary units. Using 3-CP as a concentration standard, the 100 A.U. for the adduct yields from 100 μM Fe^{2+}-200 μM H_2O_2, are about 5.5 μM POBN adduct in DMSO oxidation and 7.3 μM POBN adduct in EtOH oxidation. The ordinate at 0 μM Fe^{2+} is the background EPR spectrum. Values are expressed as means ± sd (n = 3).

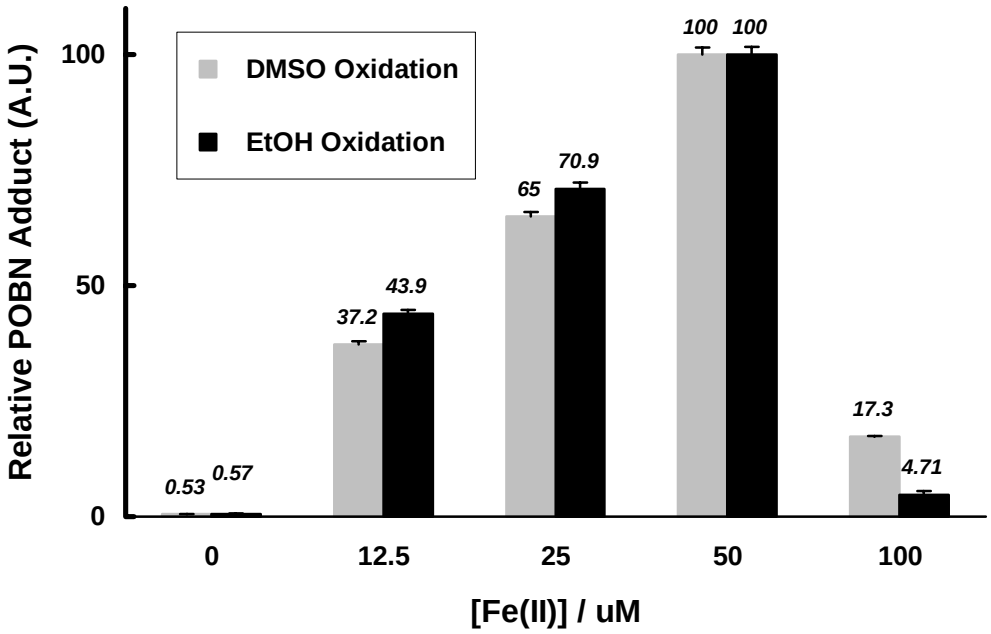

Figure 8. POBN adduct yield *vs.* $[Fe^{2+}]$ in chemical oxidations that are mediated by the anaerobic Fenton reaction ($[Fe^{2+}] > [H_2O_2]$). 100 μM DMSO or EtOH oxidized by 50 μM H_2O_2 and 0-100 μM Fe^{2+}. The ordinate represents the POBN adduct yield in arbitrary units. Using 3-CP as a concentration standard, the 100 A.U. for the adduct yields from 50 μM H_2O_2 and 50 μM Fe^{2+}, are about 3.9 μM POBN adduct in DMSO oxidation and 4.9 μM POBN adduct in EtOH oxidation. The ordinate at 0 μM Fe^{2+} is the background EPR spectrum. Values are expressed as means ± sd (n = 3).

and thereby help to identify the effective mechanism(s) in the initiation of these chemical oxidations.

POBN Spin Adducts are Formed *via* the Aerobic Fenton Reaction

In aerobic conditions, two oxygen-mediated reactions need to be considered. First, oxygen reacts with Fe^{2+} to form iron-oxygen complexes, such as ferryl or perferryl ions. These complexes can replace $^{\bullet}OH$ as the oxidant in reactions 44 and 45 in initiating chemical free radical oxidations. Second, oxygen either reacts with $^{\bullet}CH_3$ during DMSO oxidation or reacts with $CH_3{}^{\bullet}CHOH$ during EtOH oxidation to form methylperoxyl ($^{\bullet}OOCH_3$) and $^{\bullet}OOCH(CH_3)OH$ radicals, respectively. These peroxyl radicals also can be trapped by POBN, but the reaction is slow and the spin adducts are unstable. The poor trapping and fast decay of these spin adducts result in EPR detectable signals in aerobic conditions that are much smaller than those observed in anaerobic conditions. Using the central doublet of the EPR spectra (Figure 6) to determine the amount of spin adduct formation, the different yields between aerobic and anaerobic oxidation of DMSO/EtOH are shown in Table 1.

During DMSO oxidation, the methylperoxyl radical ($^{\bullet}OOCH_3$) also undergoes reactions 33 and 34 to form an alkoxyl radical ($^{\bullet}OCH_3$). Alkoxyl radical can react with POBN (reaction 35) to form a quite spin adduct detectable by EPR. This oxygen-centered radical adduct (POBN/$^{\bullet}OCH_3$) with hyperfine splitting constants: $a^N \approx 14.8$ G; $a^H \approx 2.40$ G, has an EPR spectrum morphology similar to the carbon-centered radical adduct of Figure 6-a. However, since two spin adducts are visualized under aerobic Fenton

Table 1. Comparison of POBN Adduct Yield *via* (An)Aerobic Fenton Reaction in Chemical Oxidation

[Fe(II)] with 100 μM H_2O_2		[POBN/Adduct][a] /(μM) in DMSO Oxidation	[POBN/Adduct] /(μM) in EtOH Oxidation
25 μM	N_2[b]	2.01 ± 0.09[c]	2.80 ± 0.09
	Air[d]	0.31 ± 0.02**	0.70 ± 0.07**
50 μM	N_2	3.92 ± 0.04	5.46 ± 0.16
	Air	0.56 ± 0.02**	1.36 ± 0.08**
100 μM	N_2	5.30 ± 0.05	7.10 ± 0.12
	Air	0.82 ± 0.06**	2.22 ± 0.09**

a: POBN adduct yield was quantified by using 3-CP standard.
b: control group, anaerobic system obtained by N_2 deoxygenation.
c: data are expressed as means ± sd from n = 3.
d: aerobic system (air-saturated solution).
**: $p < 0.001$ compared with control.

reaction-mediated DMSO oxidation, the final EPR spectrum (Figure 6-b) was more complex than the EPR spectrum with only one adduct, *i.e.* the EPR spectrum obtained by the authentic Fenton-mediated DMSO oxidation or obtained from EtOH oxidation (Figure 6-a).

During EtOH oxidation, only one adduct could be detected by EPR, *i.e.* POBN/$CH_3^{\bullet}CHOH$. Thus, EPR spectrum (Figure 6-a) with $a^N \approx 15.8$ G and $a^H \approx 2.7$ G will be obtained from EtOH oxidation either initiated by the anaerobic Fenton reaction or initiated by the aerobic Fenton reaction.

Under aerobic Fenton conditions, POBN spin adduct yield *vs*. [Fe^{2+}] in DMSO/EtOH oxidation is shown in Figure 9. Unlike Figure 7, 1:1 stoichiometry for POBN adduct and [Fe^{2+}] did not hold well with any [Fe^{2+}] in DMSO/EtOH anaerobic Fenton-mediated free radical oxidations. This difference implies that the role of the Fenton reagents in initiation of chemical oxidation varied with the oxygenation conditions. Under aerobic conditions, the Fenton reagents not only undergo the traditional Fenton reaction, but they also undergo other reactions to mediate chemical oxidations. To examine this possibility, the two chemical targets were also exposed to Fe^{2+} solutions or Fe^{2+}-CAT solutions. We assume that Fe^{2+}-CAT solutions initiate authentic iron-oxygen complex-mediated reactions since CAT eliminates H_2O_2. The stochiometry of iron-oxygen complex-mediated chemical oxidations is presented following.

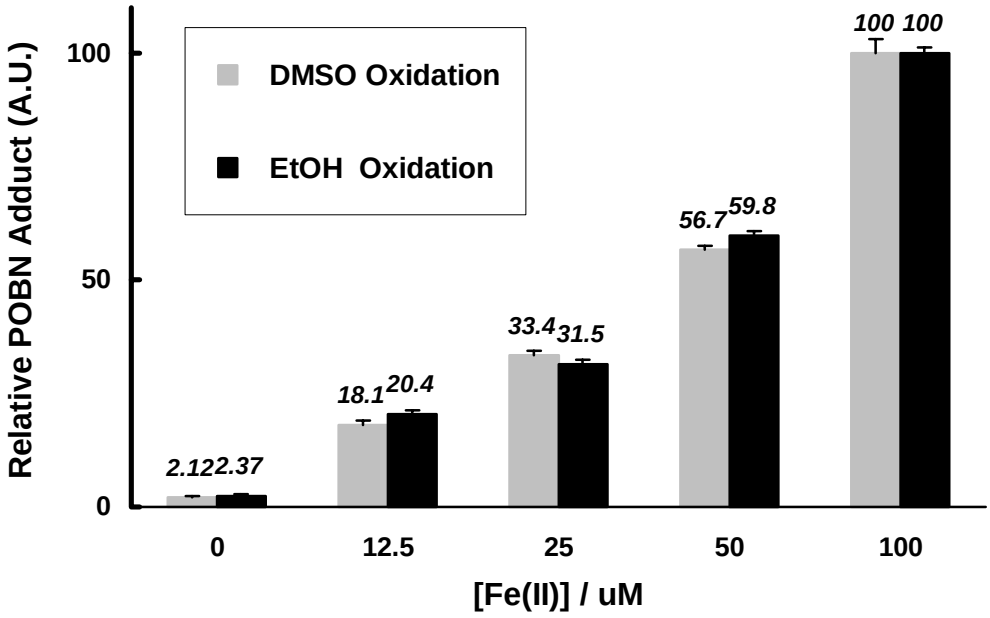

Figure 9. POBN adduct yield *vs*. [Fe^{2+}] in chemical oxidations that are mediated by aerobic Fenton reaction. 100 mM DMSO or EtOH oxidized by 200 μM H_2O_2 and 0-100 μM Fe^{2+}. The ordinate represents the POBN adduct yield in arbitrary units. Using 3-CP as a concentration standard, the 100 A.U. for the adduct yield from 100 μM Fe^{2+}-200 μM H_2O_2, are about 0.79 μM POBN adduct in DMSO oxidation and 2.3 μM POBN adduct in EtOH oxidation. The ordinate at 0 μM Fe^{2+} is the background EPR spectrum. Values are expressed as means ± sd (n = 3).

POBN Spin Adducts are Formed *via* Fe^{2+} or Fe^{2+}/CAT Initiated Oxidation

Except when H_2O_2 was omitted or H_2O_2-related enzymes, such as SOD and CAT, were added, the incubation conditions of these experiments were identical to previous experiments. Without preexisting H_2O_2, Fe^{2+} can freely initiate chemical free radical oxidations (Figure 10). Furthermore, when 500 U/ml CAT were added to make H_2O_2-free solutions, POBN spin adduct formation was only slightly inhibited; the addition of 50 U/ml SOD, rather than enhancing the POBN spin adduct formation, also slightly inhibited both chemical target oxidations just like CAT (Table 2). These results suggest that pre-existing H_2O_2 is not necessary for initiating chemical free radical oxidations, *i.e.* the Fenton reaction may not be involved in Fe^{2+}-O_2-mediated oxidation. If the Fenton reaction were involved in Fe^{2+} aerobic oxidation, then the addition of SOD and CAT should have opposite effects on these chemical oxidations due to their different effects on H_2O_2 — SOD would increase H_2O_2; CAT would decrease H_2O_2. The possibility of a nonspecific protein effect was examined by including BSA at the same protein concentration as that of SOD plus CAT in experimental incubation. The results shown in Table 2 demonstrate that the SOD and CAT results are not due to a nonspecific protein effect. Thus, we suggest that iron-oxygen complexes should have a significant role in the initiation of chemical oxidations; SOD or CAT may inhibit chemical oxidations *via* the same route, *i.e.* remove the reagent ($O_2^{\bullet -}$) for formation iron-oxygen complexes. This enzyme-mediated mechanism can be further demonstrated by adding both enzymes. As shown in Table 2, SOD and CAT significantly blunt these chemical oxidations.

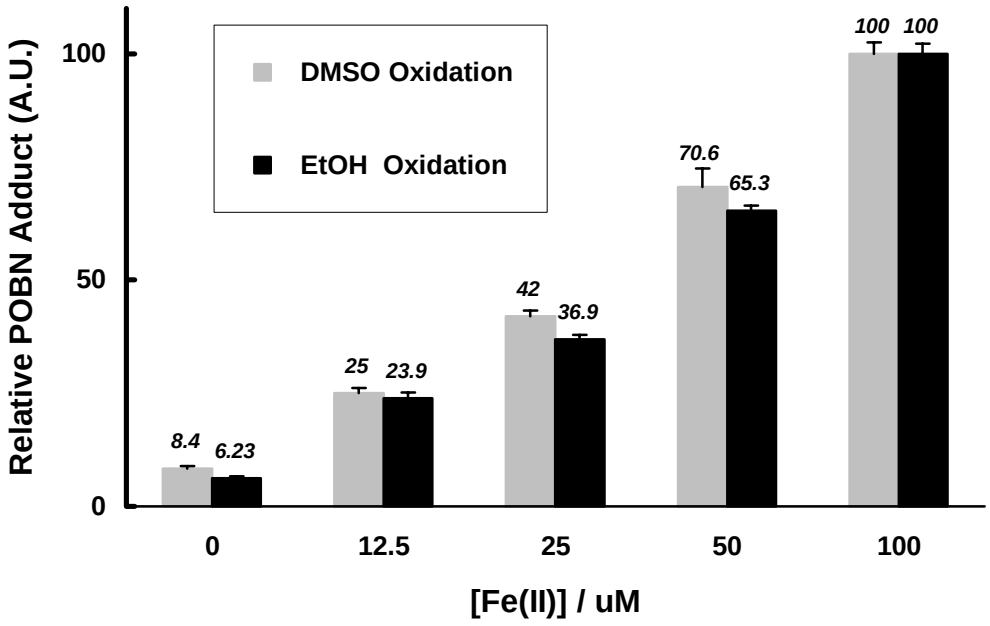

Figure 10. POBN adduct yield *vs.* [Fe^{2+}] in chemical oxidations that are mediated by aerobic Ferrous iron solution. 100 mM DMSO or EtOH was oxidized by 0-100 μM Fe^{2+}. The ordinate represents the POBN adduct yield in arbitrary units. Using 3-CP as a concentration standard, the 100 A.U. for the adduct yield from 100 μM Fe^{2+}, are 0.20 μM POBN adduct for DMSO oxidation and 0.29 μM POBN adduct for EtOH oxidation. The ordinate at 0 μM Fe^{2+} is the background EPR spectrum. Values are expressed as means ± sd (n = 3).

Table 2. Enzymes affect POBN spin adducts in chemical oxidations

100 μM Fe(II) and	[POBN/Adduct][a] /(nM) in DMSO Oxidation	[POBN/Adduct] /(nM) in EtOH Oxidation
Fe(II) alone[b]	200 ± 13.5[c]	290 ± 12.5
Fe(II) and BSA[d]	190 ± 30	280 ± 23
Fe(II) and 50 U/mL SOD	142 ± 16*	191 ± 33*
Fe(II) and 500 U/mL CAT	171 ± 17	209 ±18*
Fe(II) and SOD + CAT	100 ± 11**	120 ± 9**

a: POBN adduct yield was quantified by using 3-CP standard.
b: control group.
c: data are expressed as means ± sd from n = 3.
d: BSA at the same protein concentration of SOD + CAT.
*: $p < 0.05$ compared with control.
**: $p < 0.001$ compared with control.

As expected, the POBN adduct yield *vs.* $[Fe^{2+}]$ in iron-mediated DMSO/EtOH oxidation (Figure 10) differed from either the relationship of the anaerobic Fenton oxidation (Figure 7) or the relationship of the aerobic Fenton oxidation (Figure 9). These findings imply that under aerobic conditions Fenton reagents undergo both reactions, *i.e.* the Fenton and the iron-oxygen complex reactions, to initiate DMSO and EtOH free radical oxidations.

In biological systems, however, the oxygen needed for iron-oxygen complex-mediated oxidation mechanisms is present at a much higher concentration than $[H_2O_2]_{ss}$ for the Fenton reaction-mediated mechanism. We estimate that the $[O_2]_{ss}/[H_2O_2]_{ss}$ in living systems is on the order of 10^5 [25, 26]. Thus, we examined the efficiency of the classical Fenton reaction in initiation of chemical free radical oxidations and compared to the initiation efficiency of iron-oxygen complexes.

Fenton Efficiency Varies with $[O_2]/[H_2O_2]$ Ratio in Chemical Oxidations

Under various experimental $[O_2]/[H_2O_2]$, we compared the POBN spin adduct yield of the aerobic Fenton reaction-mediated oxidation *vs*. adduct yield of the Fe^{2+} aerobic reaction-mediated oxidation. From these relative spin adduct yields *, we can infer the relative efficiency of the Fenton reaction *vs*. the iron-oxygen complex reactions in the initiation of chemical oxidations.

---

* If initial $[O_2]$ is assumed as 250 μM for aerobic, the relative yield of POBN adduct

$$= \frac{([\text{POBN/adduct}] \text{ from } Fe^{2+} \text{ in the presence of } H_2O_2 \text{ and } O_2)}{([\text{POBN/adduct}] \text{ from } Fe^{2+} \text{ in the presence } O_2 \text{ only})}$$

In Figures 11 and 12, the abscissa represents the experimental $[O_2]/[H_2O_2]$; and the ordinate represents the relative yield of POBN adduct, *i.e*. yield of Fenton-mediated oxidation *vs.* yield of aerobic Fe^{2+}-mediated oxidation. As shown in these Figures, the efficiency of the Fenton reaction in both oxidations varies greatly with $[O_2]/[H_2O_2]$ and is related to $[Fe^{2+}]$. The Fenton efficiency varies greatly with $[O_2]/[H_2O_2]$ at high $[Fe^{2+}]$. For example, the Fenton efficiency of 100 μM Fe^{2+}-mediated EtOH oxidation can vary from high (ordinate ≈ 8 in Figure 12) at $[O_2]/[H_2O_2] \approx 1$ to low (ordinate ≈ 1 in Figure 12) at $[O_2]/[H_2O_2] \approx 100$. The Fenton efficiency for DMSO oxidation with 100 μM Fe^{2+} varied from ordinate ≈ 4 at $[O_2]/[H_2O_2] \approx 1$ to ordinate ≈ 1 at $[O_2]/[H_2O_2] \approx 100$ (Figure 11). However, at low Fe^{2+}, the ordinate value is always small no matter the $[O_2]/[H_2O_2]$ especially in DMSO oxidation. These results imply that the Fenton reaction appears to be a minor initiator compared to the iron-oxygen complexes, *i.e.* iron-oxygen complexes contribute most to the adduct yield under low $[Fe^{2+}]$ and/or high $[O_2]/[H_2O_2]$.

Based on an estimated physiological $[O_2]/[H_2O_2]$ of 10^5, we strongly suggest that the Fenton reaction, using preexisting H_2O_2, is only a minor initiator; iron-oxygen complexes may be significant, unappreciated initiators of free radical oxidations.

From the data of Figures 11 and 12 we also find that the Fenton reaction seems to be of different significance in the initiation of DMSO and EtOH oxidations. If high $[Fe^{2+}]$ and low $[O_2]/[H_2O_2]$ were used to initiate chemical oxidations, the Fenton reaction in EtOH oxidation always had higher efficiency than the Fenton reaction in DMSO oxidation. For example, $[O_2]/[H_2O_2] \approx 1$, ordinate ≈ 8 for EtOH and ordinate ≈ 4 for

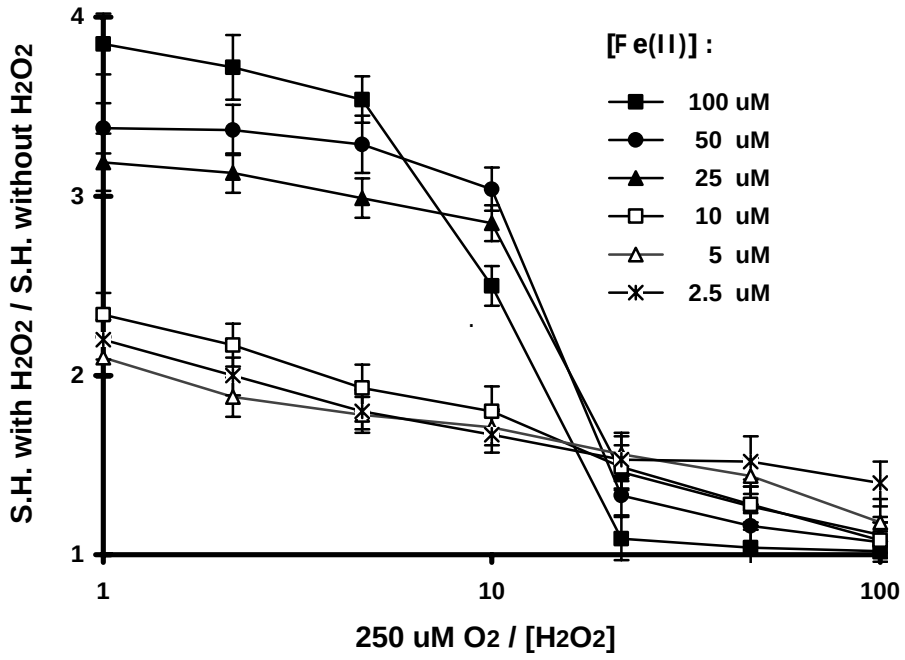

Figure 11. Relative Fenton efficiency of DMSO oxidation. 100 mM DMSO was incubated with 2.5, 5, 10, 25, 50, and 100 μM Fe^{2+} with/without 2.5, 5, 10, 25, 50, 100, and 250 μM H_2O_2 under aerobic conditions. All solutions were air-saturated, thus initial $[O_2] \approx 250$ μM. Values were expressed as means ± sd (n = 3) .

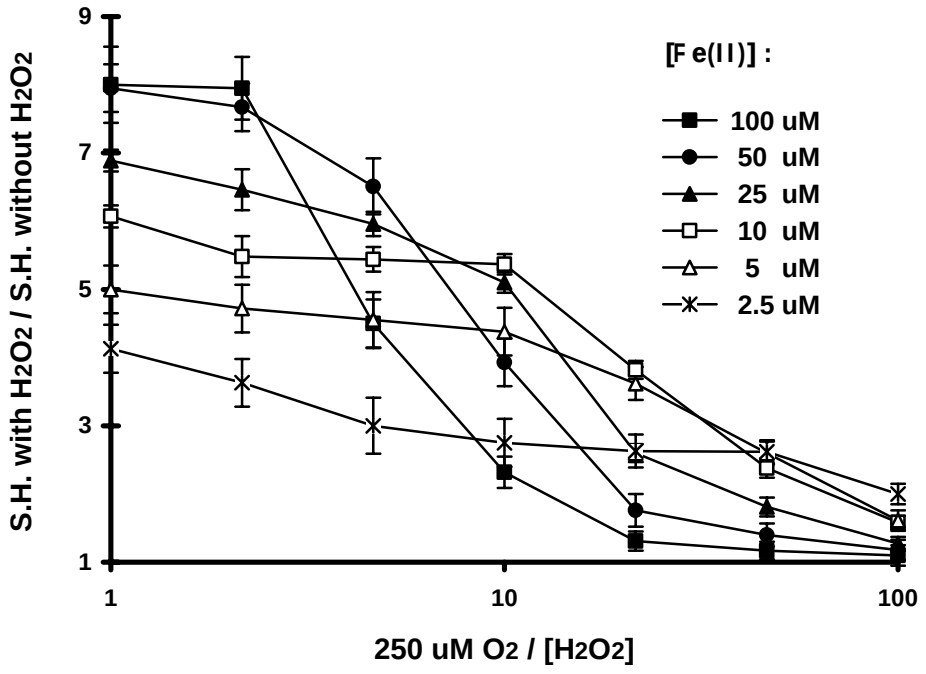

Figure 12. Relative Fenton efficiency of EtOH oxidation. 100 mM EtOH was incubated with 2.5, 5, 10, 25, 50, and 100 μM Fe^{2+} with/without 2.5, 5, 10, 25, 50, 100, and 250 μM H_2O_2 under aerobic conditions. All solutions were air-saturated, thus initial $[O_2] \approx 250$ μM. Values were expressed as means ± sd (n = 3).

DMSO. These results could be attributed to the different trapping efficiency of POBN for DMSO and EtOH; but it is also possible for that the Fenton reaction may play a more important role in EtOH oxidation than in DMSO oxidation. In the next set of experiments, we address the relationship of the Fenton reaction efficiency and the experimental model.

Fenton Reagents Affect Chemical Free Radical Oxidations Differently

In the anaerobic Fenton reaction, excess Fe^{2+} may destroy the POBN spin adduct formed from Fenton-mediated oxidations (Figure 8). However, this effect disappeared when the Fenton reaction is initiated in aerobic conditions (Figure 13). This difference suggests again that iron-oxygen complexes play a significant role in the aerobic Fenton system, because excess ferrous iron did not destroy the POBN adduct, but stimulated POBN adduct formation by the formation of iron-oxygen complexes.

If we accept that the stochiometry of H_2O_2 and Fe^{2+} for the Fenton reaction is 1:1 [40], then the POBN adduct yield should have similar stochiometry either oxidized by varied [Fe^{2+}] with fixed [H_2O_2] or by varied [H_2O_2] with fixed [Fe^{2+}]. As shown in Figure 14, the relative POBN adduct yields have very similar shapes when EtOH was oxidized by varied [Fe^{2+}] and fixed [H_2O_2] or by varied [H_2O_2] and fixed [Fe^{2+}]. This result implies that both Fenton reagents affect EtOH oxidations similarly. However, in DMSO oxidation (See Figure 15) the stochiometric curve of POBN adduct yield by fixed [Fe^{2+}] significantly differs from the curve for fixed [H_2O_2]; increasing [Fe^{2+}] always enhances POBN adduct yield in DMSO oxidation. This result implies that iron-oxygen

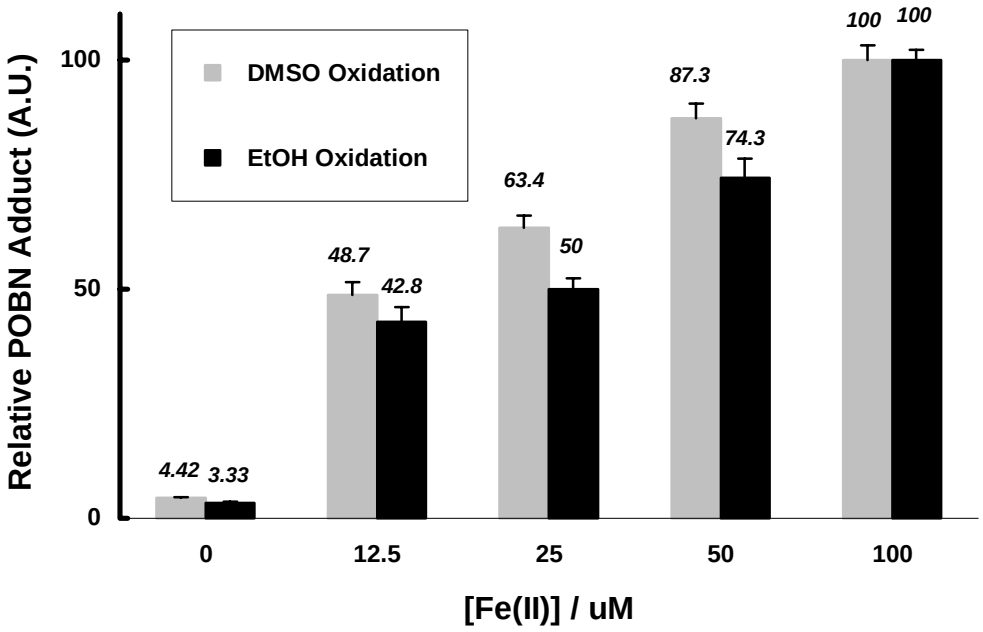

Figure 13. POBN adduct yield *vs*. [Fe^{2+}] in chemical oxidations that are mediated by aerobic Fenton reaction ([Fe^{2+}] > [H_2O_2]). 100 μM DMSO or EtOH oxidized by 50 μM H_2O_2 and 0-100 μM Fe^{2+}. The ordinate represents the POBN adduct yield in arbitrary units. Using 3-CP as a concentration standard, the 100 A.U. for the adduct yield from 50 μM H_2O_2 and 50 μM Fe^{2+}, are about 0.59 μM POBN adduct in DMSO oxidation and 1.3 μM POBN adduct in EtOH oxidation. The ordinate at 0 μM Fe^{2+} is the background EPR spectrum. Values are expressed as means ± sd (n = 3).

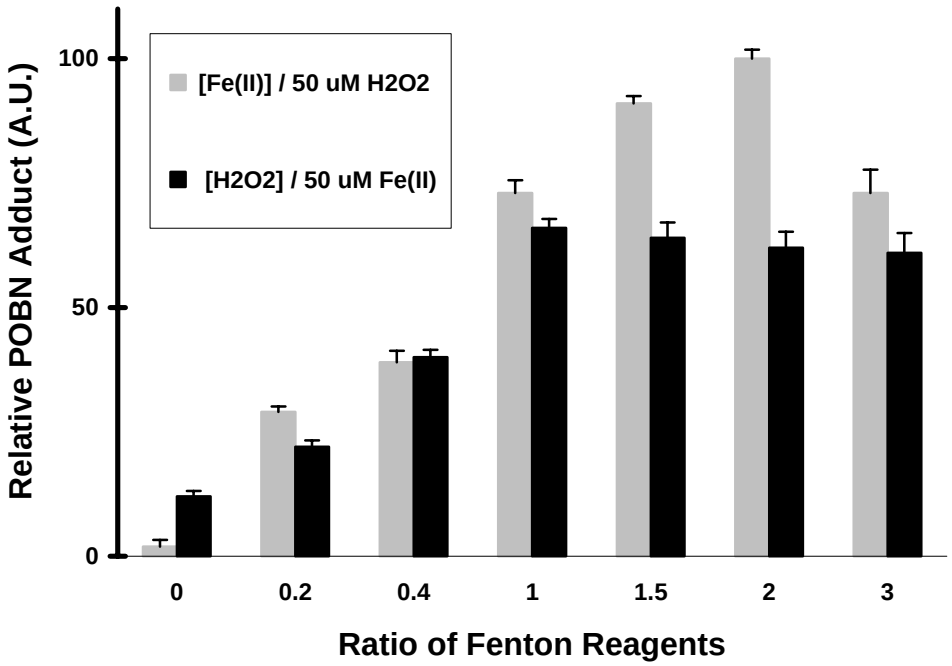

Figure 14. Fenton reagents *vs*. POBN adduct yield in EtOH oxidation. EtOH oxidized by 50 μM Fe^{2+} with 0, 10, 20, 50, 75, 100, 150 μM H_2O_2; and 50 μM H_2O_2 with 0, 10, 20, 50, 75, 100, 150 μM Fe^{2+}. Using 3-CP as a concentration standard, 100 A.U. ≈ 2.2 μM POBN adduct. The ordinate for $[Fe^{2+}]/[H_2O_2] = 0$ was the EPR background spectrum. Values are expressed as means ± sd (n = 3).

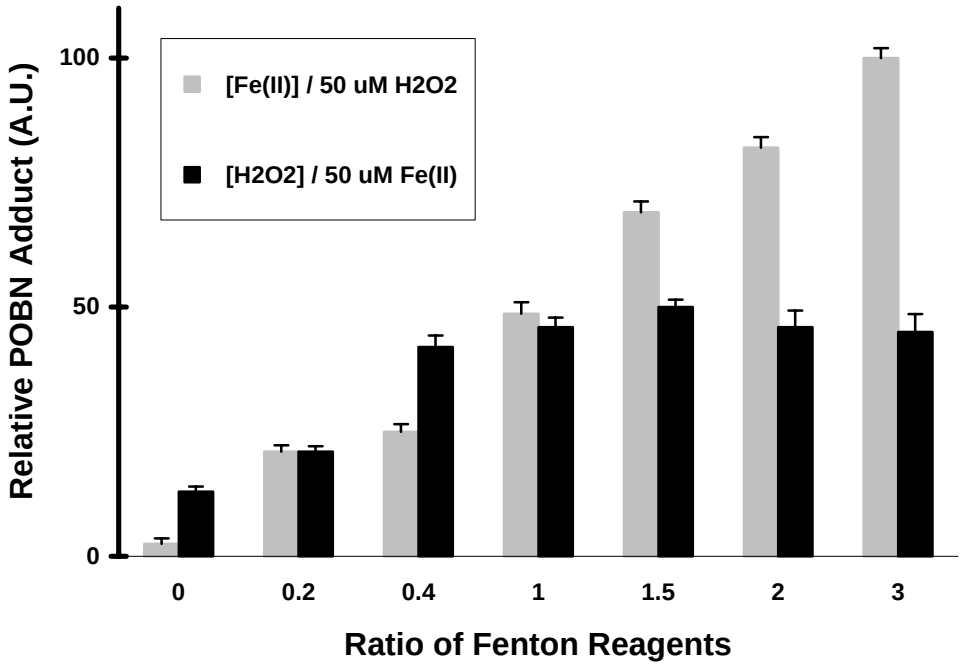

Figure 15. Fenton reagents *vs*. POBN adduct yield in DMSO oxidation. DMSO oxidized by 50 μM Fe^{2+} with 0, 10, 20, 50, 75, 100, 150 μM H_2O_2; and 50 μM H_2O_2 with 0, 10, 20, 50, 75, 100, 150 μM Fe^{2+}. Using 3-CP as a concentration standard, 100 A.U. ≈ 1.3 μM POBN adduct. The ordinate for $[Fe^{2+}]/[H_2O_2] = 0$ was the EPR background spectrum. Values are expressed as means ± sd (n = 3)

complexes are significant species in initiation of DMSO oxidation.

Based on these observations, we suggest that the Fenton reaction plays a lesser role in DMSO oxidation than it does in EtOH oxidation. The possible interpretation is that hydroxyl radical in DMSO oxidation might undergo two types of reactions: hydrogen abstraction and an addition reaction to a double bond. However, the addition reaction can not occur in EtOH oxidation. We suggest that the occurrence of hydroxyl radical addition reactions might overwhelm its abstracting reaction from unsaturated compounds, such as lipid fatty acid chain. Therefore, the hydrogen abstraction reaction, *i.e.* initiation of free radical oxidations, is mainly induced by iron-oxygen complexes rather than hydroxyl radical. Thus, iron-oxygen complexes have an unappreciated role in initiating all free radical oxidations.

Fenton-Mediated Chemical Oxidations Consume H_2O_2 Differently

Chemical targets (100 mM) exposed to 25 μM H_2O_2 and 0, 25, 37.5, 50, or 75 μM Fe^{2+} were used to measure how much H_2O_2 remained after the Fenton reaction occurred. The H_2O_2 was estimated by using an oxygen monitor to measure the O_2 produced by reaction 43.

$$2\ H_2O_2 \xrightarrow{\text{CAT}} O_2 + 2H_2O \qquad (43)$$

According to our observations (Table 3), no H_2O_2 remains when DMSO is oxidized by $[Fe^{2+}]/[H_2O_2] \approx 3{:}1$. However, in EtOH oxidation, the $[Fe^{2+}]/[H_2O_2]$ ratio that consumed all H_2O_2 was only 2:1. The differing H_2O_2 depletion observed in DMSO and EtOH oxidations suggests that Fenton reagents affect these chemical oxidations

Table 3. H_2O_2 remaining after the Fenton reaction

Fenton Reagents		$[H_2O_2]$ Remaining (μM) after DMSO Oxidation	$[H_2O_2]$ Remaining (μM) after EtOH Oxidation
$[H_2O_2]$	[Fe(II)]		
0 μM	all[a]	0	0
25 μM	0 μM	25 ± 0.31[b]	25 ± 0.33
	25 μM	9.6 ± 0.18	6.6 ± 0.21
	37.5 μM	5.9 ± 0.17	3.3 ± 0.18
	50 μM	3.3 ± 0.16	0 ± 0.16
	75 μM	0 ± 0.16[c]	0 ± 0.16

Oxygen Monitor Experiment.

a: with no preexisting H_2O_2, no oxygen generation could be measured upon addition of CAT with all $[Fe^{2+}]$.

b: Each data point is expressed as mean ± sd (n = 3).

c: 0.16 μM is representative of the oxygen monitor background signal.

differently; the Fenton reaction appears to have a more important role in EtOH oxidation than in the DMSO oxidation, *i.e.* iron oxygen complexes play a more important role in DMSO oxidation than in EtOH oxidation.

Chelators Affect the Relative Initiation Efficiency of Chemical Oxidations

EDTA and DTPA are widely used as iron chelators in biological research because they can drastically alter the efficiency of iron as a catalyst for the Haber-Weiss reaction [41]. DTPA-Fe^{2+} and EDTA-Fe^{2+} complexes have been reported to be more efficient than Fe^{2+} in inducing the Fenton reaction [23]. The effects of EDTA and DTPA on iron autoxidation and related lipid peroxidation have also been well documented [42]. DTPA, in contrast to EDTA, has been considered to inhibit the Haber-Weiss reaction by significantly slowing $Fe^{3+} \rightarrow Fe^{2+}$ reduction.

In order to study the chelator effect on the Fenton reaction, EDTA or DTPA and Fe^{2+} were premixed under N_2 or argon to prevent the chelated iron autoxidation process. The effect of EDTA and DTPA upon Fenton reaction-mediated and iron-oxygen complex-mediated chemical oxidations are shown in Figures 16 and 17. The Fenton reaction efficiencies of unchelated iron-mediated oxidation, inferred from Bar 2 *vs*. Bar 1 in these Figures, are higher than the Fenton efficiencies of chelated iron (Bar 4 or 6 *vs*. Bar 3 or 5). In the other word, chelators greatly enhance the efficiency of iron-oxygen complexes in initiation of free radical oxidation. Furthermore, EDTA and DTPA both significantly increased iron-oxygen complex-mediated oxidation (Bar 3 or 5 *vs*. Bar 1). The chelator effect provides the convincing evidence supporting our hypothesis that iron-

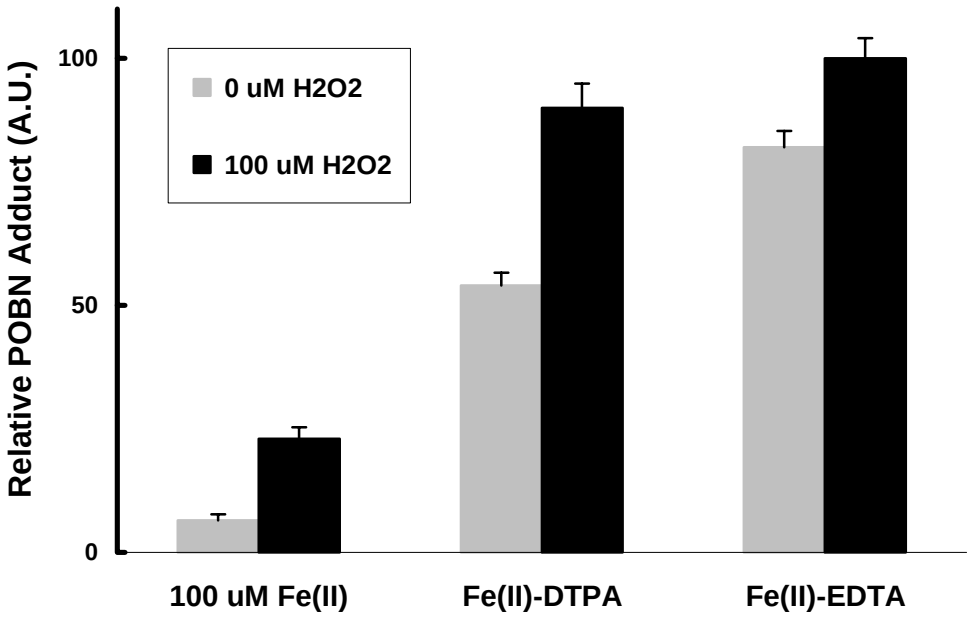

Figure 16. Chelator effect on DMSO oxidation. The ordinate represents the POBN adduct yield in arbitrary unites. Using 3-CP as a concentration standard, 100 A.U., the POBN adduct yield from 100 μM Fe^{2+}-EDTA and 100 μM H_2O_2, is about 2.5 μM POBN adduct. Counting from the left: Bar 1 to Bar 6. The chelator effects on enhancement of iron-mediated glucose oxidation were 8-fold for DTPA (bar 3), 13-fold for EDTA (bar 5), and 4-fold for H_2O_2-free iron (bar 2) higher than control (bar 1, 100 μM Fe^{2+} mediated), respectively (n=3, $p < 0.001$).

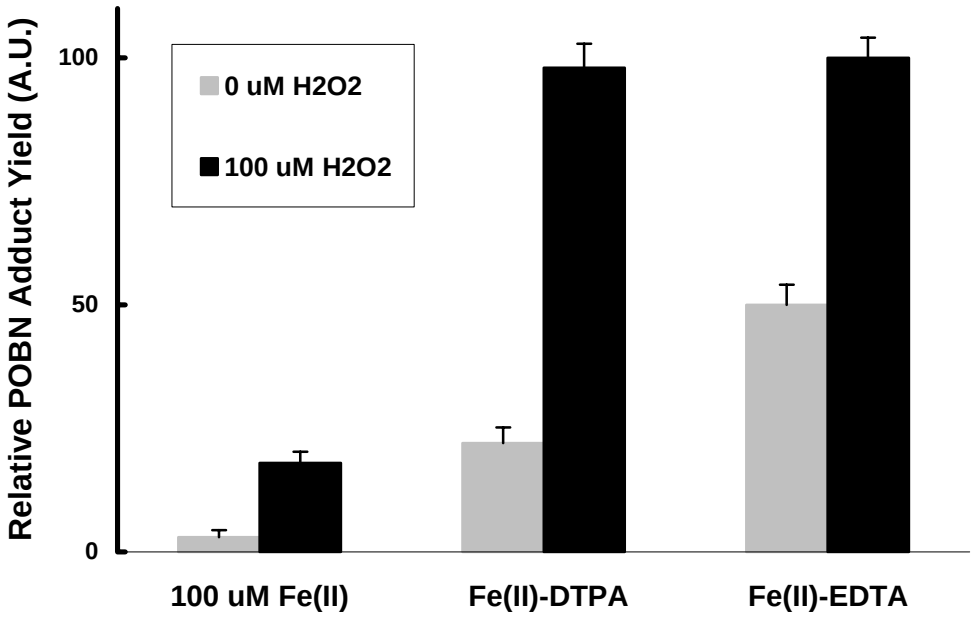

Figure 17. Chelator effect on EtOH oxidation. The ordinate represents the POBN adduct yield in arbitrary unites. Using 3-CP as a concentration standard, 100 A.U., the POBN adduct yield from 100 μM Fe^{2+}-EDTA and 100 μM H_2O_2, is about 12.7 μM POBN adduct. Counting from the left: Bar 1 to Bar 6. The chelator effects on enhancement of iron-mediated glucose oxidation were 7-fold for DTPA (bar 3), 17-fold for EDTA (bar 5), and 8-fold for H_2O_2-free iron (bar 2) higher than control (bar 1, 100 μM Fe^{2+} mediated), respectively (n=3, $p < 0.001$).

oxygen complex-mediated oxidations should have a very important role in living systems.

Conclusions of Chemical Oxidations

By using EPR spin trapping and oxygen monitor techniques to study the DMSO and EtOH free radical oxidations initiated *via* the Fenton reaction and iron-oxygen complexes reaction, we conclude that:

1) two mechanisms, *i.e.* the Fenton reaction and iron-oxygen complex reaction, are active in the initiation of DMSO and EtOH free radical oxidations;
2) the Fenton reaction efficiency varied greatly with $[O_2]/[H_2O_2]$. It decreases as $[O_2]/[H_2O_2]$ increases. For example, $[O_2]/[H_2O_2] \approx 1/1$, the Fenton reaction can initiate the oxidation of both chemical targets efficiently. However, with $[O_2]/[H_2O_2] \approx 100/1$, the Fenton reaction plays an insignificant role while iron-oxygen complexes are responsible for most POBN spin adduct formation.
3) the Fenton reaction efficiency also varied with $[Fe^{2+}]$. See Table 4.

Therefore, based on our study and extrapolating to living systems where high $[O_2]/[H_2O_2]$ ratios and low $[Fe^{2+}]$ exist, we conclude that iron-oxygen complexes have a significant role in free radical oxidations.

Table 4. Fenton efficiency *vs*. $[O_2]/[H_2O_2]$ and $[Fe^{2+}]$ in chemical oxidations

Oxidizing System		High $[Fe^{2+}]$[a]	Low $[Fe^{2+}]$
DMSO	High $[O_2]/[H_2O_2]$[b]	low[c]	low
	Low $[O_2]/[H_2O_2]$	intermediate[d]	low
EtOH	High $[O_2]/[H_2O_2]$	low	intermediate
	Low $[O_2]/[H_2O_2]$	high[e]	intermediate

a: high $[Fe^{2+}] > 25$ μM; low $[Fe^{2+}] < 25$ μM.
b: high $[O_2]/[H_2O_2] \approx 10$ -100 ($[O_2] \approx 250$ μM in aerobic condition)
c: low Fenton efficiency means ordinate in Figures 11 and $12 \leq 2$.
d: intermediate means ordinate in Figures 11 and $12 \approx 2$ - 4.
e: high means ordinate in Figures 11 and $12 \geq 4$

CHAPTER IV

BIOCHEMICAL FREE RADICAL OXIDATIONS

Results and Discussion

Two biochemical molecules, glucose and glyceraldehyde, were used in this work to probe the research question — How effective is the classical Fenton reaction in initiating biochemical free radical oxidations? The experimental models we established in the chemical oxidations were used to estimate the relative efficiency of Fenton reaction *vs.* iron-oxygen complex reaction in initiating glucose or glyceraldehyde free radical formation.

Glucose can oxidize under physiological conditions to produce highly reactive oxidants such as hydrogen peroxide and ketoaldehydes, which are reported to be able to induce substantial alterations in protein structure and function [43]. Glyceraldehyde may oxidize under physiological conditions to generate several intermediates including carbon-center free radicals, superoxide, hydrogen peroxide, and even hydroxyl radical [44]. Thus, glucose or glyceraldehyde autoxidation under physiological conditions is believed to be of pathophysiological significance, contributing to tissue damage in diabetes mellitus and aging. Particular attention has been given to these autoxidations and their effects on macromolecule alterations, *i.e.* protein fragmentation and protein

conformation alterations. In this thesis, however, we focus on the initiation role of oxidative species, such as hydroxyl radical or iron-oxygen complexes, on the formation of target molecule radicals, *i.e.* formation of glucose radicals and glyceraldehyde radicals.

Based on our observations we suggest that, similar to the chemical oxidations, the Fenton reaction plays a minor role in initiation of glucose and glyceraldehyde free radical oxidations; thus, iron-oxygen complexes should be a significant initiator for these biochemical free radical oxidations, and thereby be of physiological significance.

POBN Spin Adducts are Formed *via* Iron-Mediated Glucose Oxidation

According to the chemistry of glucose autoxidation [43] (Figure 18), the enolisation of monosaccharides to end-diol intermediates is the first step. The enediol radical anion formation during the monosaccharide's enolisation is a transition metal catalyzed reaction. The enediol radical can rapidly react with oxygen to form protein-reactive ketoaldehydes and superoxide. Superoxide then dismutes to hydrogen peroxide, and thereby serving as a Fenton reagent (box of Figure 18).

Firstly, we examined how effective is the Fenton reaction (box of Figure 18) on the initiation of glucose radical formation, *i.e.* does hydroxyl radical formed from glucose autoxidation have a significant role in initiating glucose radical formation. As shown in Figure 19-a, 100 μM [Fe^{3+}] aerobic solution can not induce detectable glucose radical adduct formation. This may result from very low H_2O_2 yield from glucose enolisation. Thus, 50 mM phosphate buffer solution was replaced by 150 mM chelated phosphate buffered solution for preparing all oxidative components to enhance glucose enolisation

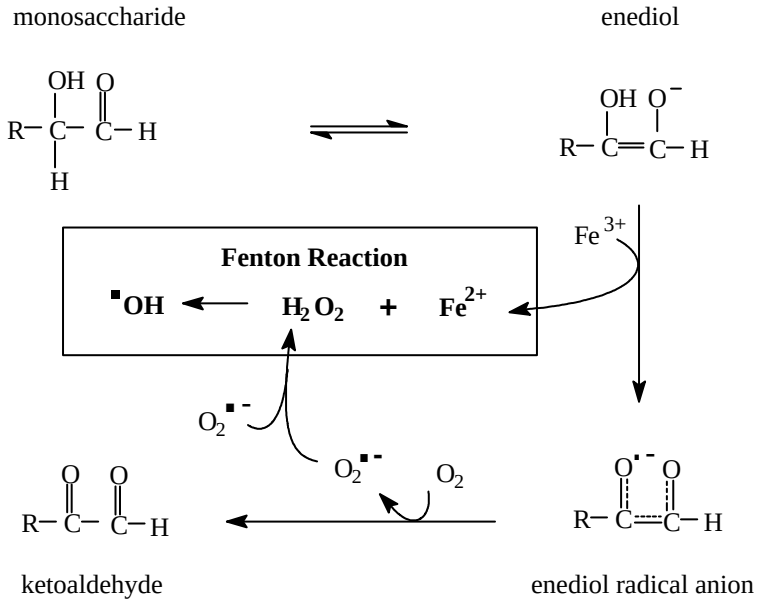

Figure 18. Scheme of glucose autoxidation [43].

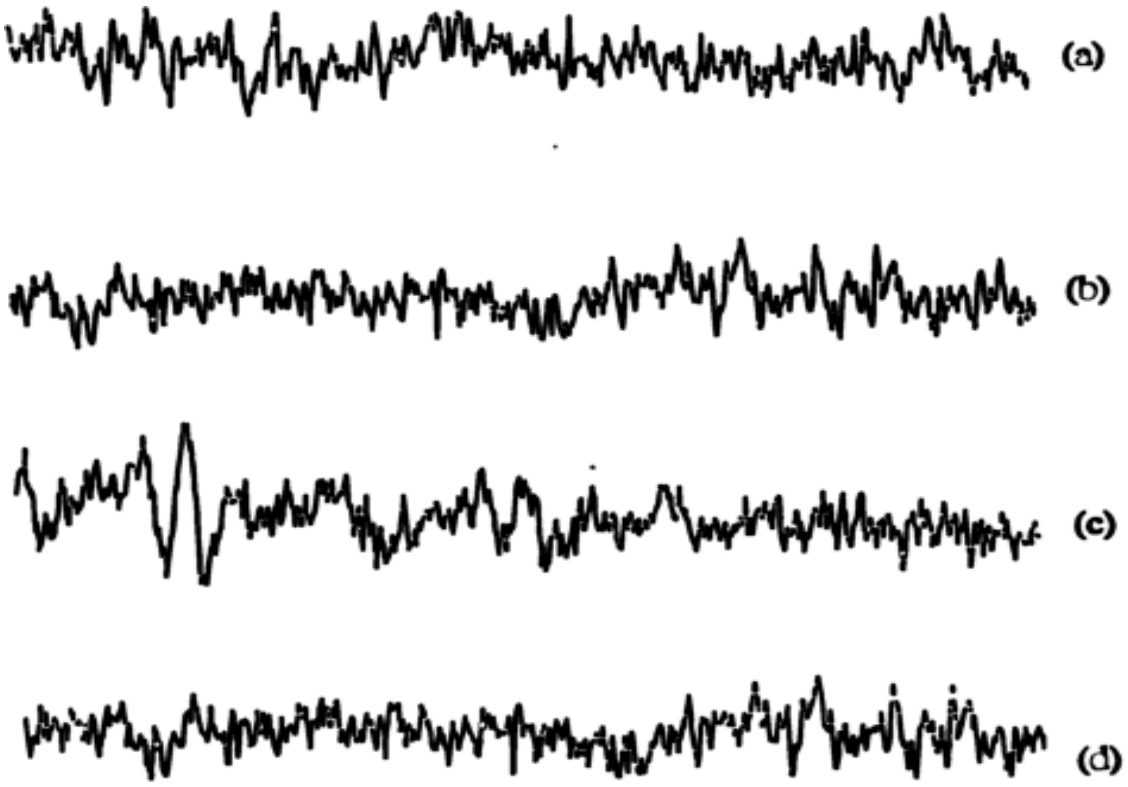

Figure 19. EPR spectrum of POBN adduct formed from Fe^{3+}(100 μM)-mediated glucose (200 mM) oxidation. 20 mM POBN was used as spin trap.

(a) 50 mM phosphate buffered solution;
(b) 150 mM phosphate buffer solution;
(c) 50 mM phosphate buffered solution with 200 μM H_2O_2;
(d) 50 mM phosphate buffered solution with 50 U/mL SOD.

rate. However, also as shown in Figure 19-b, 150 mM phosphate buffer still failed to induce any significant EPR result. In additional experiments, H_2O_2 or SOD was added to the Fe^{3+} incubation solution to further examine the significance of the Fenton reaction (box of Figure 18) in initiating glucose radical formation. Only with high H_2O_2 (200 μM), was a very unstable POBN spin adduct fleetingly detected by EPR (Figure 19-c). The addition of SOD failed to induce any EPR result (Figure 19-d). These results suggest that the box of Figure 18 appears to be an insignificant player for initiating glucose radical formation.

To further examine the efficiency of the box in Figure 18, the spin trap DMPO was used to probe if hydroxyl radical is involved in the autoxidation of glucose. Incubating glucose with 100 μM Fe^{3+} and 25 mM DMPO, neither DMPO/$^{\bullet}$OH nor DMPO carbon radical adducts were detected (Figure 20-a). The standard EPR spectrum of DMPO/$^{\bullet}$OH has splitting constants: $a^N \approx a^H \approx 14.9$ G shown in Figure 20-b. Failure to detect DMPO/$^{\bullet}$OH implies again that the box of Figure 18 has an insignificant role in glucose radical formation; furthermore, it is questionable the reaction in the box of Figure 18 can mediate significant glucose radical formation.

When 100 mM glucose was incubated with Fe^{2+} under aerobic condition, the glucose radical formation can be measured by EPR spin trapping with POBN. The chemical mechanism of this process shows as following:

$$\text{Glucose} \xrightarrow{[O]} {}^{\bullet}\text{Glucose} \xrightarrow{\text{POBN}} \text{POBN}/{}^{\bullet}\text{Glucose} \qquad (47)$$

The EPR spectra of glucose radical adduct has a typical carbon radical spectra

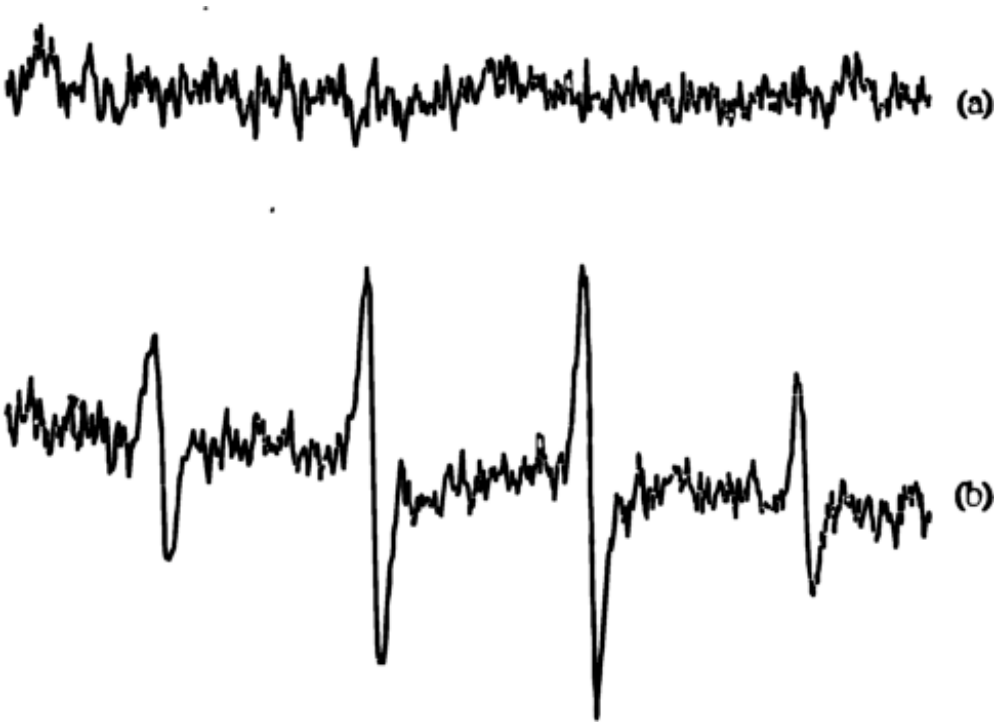

Figure 20. EPR spectrum of DMPO adduct.
(a) incubating 100 mM glucose with 20 mM DMPO and 100 μM Fe^{2+};
(b) 20 mM DMPO with Fenton reagents (Fe^{2+}-H_2O_2).

with hyperfine splitting constants: $a^N \approx 15.6$ G, $a^H \approx 2.4$ G. According to the glucose chemistry (Figure 21), the most probable radical formed in glucose oxidation is the glucopyranose radical. This radical is formed by dissociation of the anomeric C-H bond of glucopyranose.

500 U/mL CAT and 50 U/mL SOD were added to glucose-ferrous solution to examine if the Fenton reaction involved in Fe^{2+}-O_2-mediated oxidation. BSA was used as a control to examine the possibility of nonspecific protein effects. As shown in Table 5, SOD and CAT slightly inhibit the yield of glucose radical. If we assume that $^{\bullet}OH$ is involved in Fe^{2+} aerobic glucose oxidation, SOD would enhance glucose radical formation *via* catalyzing $O_2^{\bullet-}$ dismutasion to form H_2O_2, while CAT would inhibit glucose radical formation by decomposing H_2O_2 to H_2O and O_2. Thus, Table 5 demonstrates that iron-oxygen complexes rather than $^{\bullet}OH$ play a significant role in the formation of glucose radical; SOD and CAT both can inhibit glucose radical formation by directly or indirectly decreasing the required reagent ($O_2^{\bullet-}$) needed in forming iron-oxygen complexes.

Fenton Efficiency Varies with $[O_2]/[H_2O_2]$ Ratio in Glucose Oxidation

To further examine the significance of the Fenton reaction in initiation of glucose radical formation, POBN spin adduct yield from aerobic Fe^{2+}-H_2O_2-mediated oxidation was compared with POBN spin adduct yield from aerobic Fe^{2+}-mediated oxidation under the various experimental $[O_2]/[H_2O_2]$. In Figure 22, the abscissa represents the experimental $[O_2]/[H_2O_2]$; and the ordinate represents the relative yield of POBN adduct,

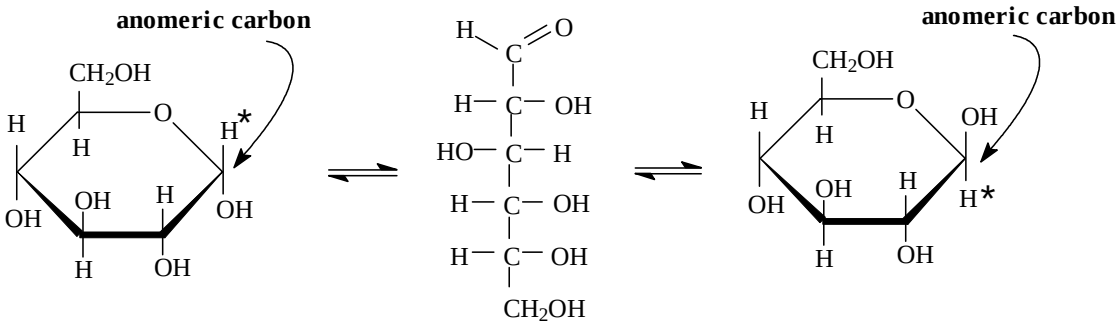

α-D-Glucopyranose D-Glucose β-D-Glucopyranose

Figure 21. Glucose structure. The pyranose sugars interconvert through the linear form of D-glucose and differ only by the configurations about their anomeric carbon atoms. The H marked by * is dissociated from anomeric carbon during glucose oxidation.

Table 5. Enzymes affect POBN spin adducts in glucose oxidation

100 μM Fe(II) and	[POBN/Adduct]/(nM)[a] in Glucose Oxidation
Fe(II) alone[b]	33.0 ± 2.0[c]
Fe(II) and BSA[d]	31.7 ± 1.5
Fe(II) and 50 U/mL SOD	28.8 ± 1.8
Fe(II) and 500 U/mL CAT	30.1 ± 1.7
Fe(II) and SOD + CAT	21.6 ± 1.6*

a: POBN adduct yield was quantified by using 3-CP standard.
b: control.
c: data are expressed as mean ± sd form n = 3.
c: BSA at the same protein concentration as SOD + CAT.
*: $p < 0.05$ compared with control.

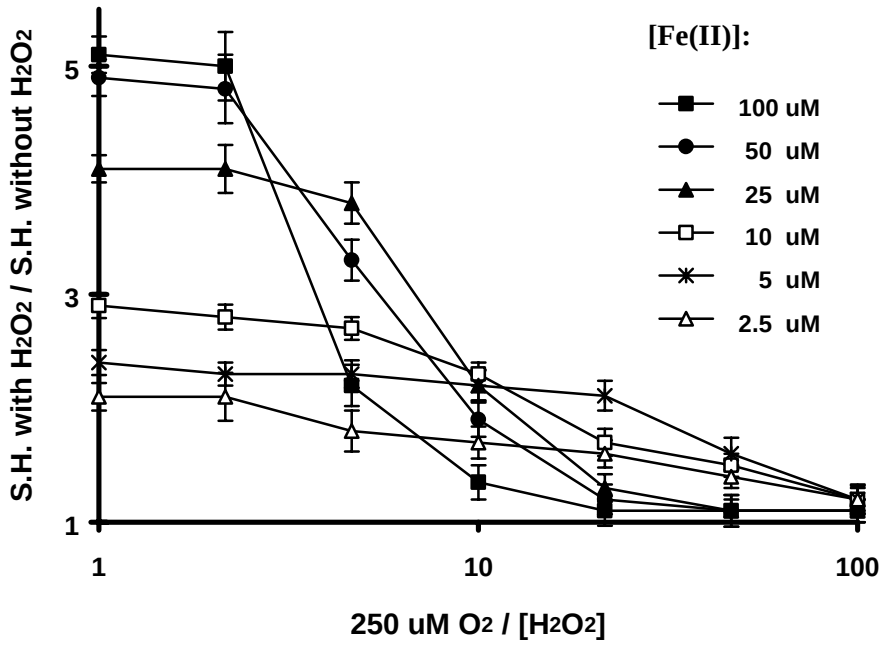

Figure 22. Relative Fenton efficiency of glucose oxidation. 200 mM glucose was incubated with 2.5, 5, 10, 25, 50, and 100 μM Fe^{2+}; with/without 2.5, 5, 10, 25, 50, 100, and 250 μM H_2O_2 under aerobic condition. All solutions were air-saturated, thus initial $[O_2] \approx 250$ μM. Values are expressed as mean ± sd (n = 3) .

i.e. yield of Fenton-mediated oxidation *vs*. yield of aerobic ferrous-mediated oxidation.

As shown in Figure 22, the efficiency of the Fenton reaction in glucose oxidation varies

with $[O_2]/[H_2O_2]$ and $[Fe^{2+}]$. There is a close similarity with DMSO (Figure 11). Thus, we suggest that Fenton-mediated glucose oxidation, like DMSO oxidation, is predominately initiated by iron-oxygen complexes rather than $^{\bullet}OH$ radical from pre-existing H_2O_2, especially under physiological conditions in which low $[Fe^{2+}]$ and high $[O_2]/[H_2O_2]$ exist. The $[O_2]/[H_2O_2]$ as well as $[Fe^{2+}]$ dependence of relative Fenton efficiency are presented in Table 6.

Chelator Affect the Relative Initiation Efficiency of Glucose Oxidation

Similar to the effect of chelated iron in DMSO and EtOH oxidations, we find that the Fenton reaction efficiency, estimated by comparing the spin adduct yield with H_2O_2 *vs.* spin adduct yield without H_2O_2, was decreased significantly from free iron (higher Fenton efficiency: Bar 2 *vs*. Bar 1 in Figure 23) to chelated iron (lower Fenton efficiency: Bar 4 or 6 *vs*. Bar 3 or 5 in Figure 23). Without preexisting H_2O_2, furthermore, chelated iron can enhance the glucose radical formation more efficiently than free iron does (compare bar 3 or 5 with bar 1). Thus, the chelator effect in glucose oxidation supports the following conclusion: iron-oxygen complexes rather than $^{\bullet}OH$ radical play a significant role in initiation of glucose free radical oxidation, and thereby being of physiological significance.

Table 6. Fenton efficiency *vs*. $[Fe^{2+}]$ as well as $[O_2]/[H_2O_2]$

in glucose oxidation

Oxidizing System	High $[Fe^{2+}]$[a]	Low $[Fe^{2+}]$
High $[O_2]/[H_2O_2]$[b]	low[c]	low
Low $[O_2]/[H_2O_2]$	intermediate[d]-high[e]	low- intermediate

a: high $[Fe^{2+}] > 25$ μM; low $[Fe^{2+}] < 25$ μM.
b: high $[O_2]/[H_2O_2] \approx 10$ -100 ($[O_2] \approx 250$ μM in aerobic condition)
c: low Fenton efficiency means ordinate in Figure 22 ≤ 2.
d: intermediate means ordinate in Figure 22 ≈ 2 - 4.
e: high means ordinate in Figure 22 ≥ 4

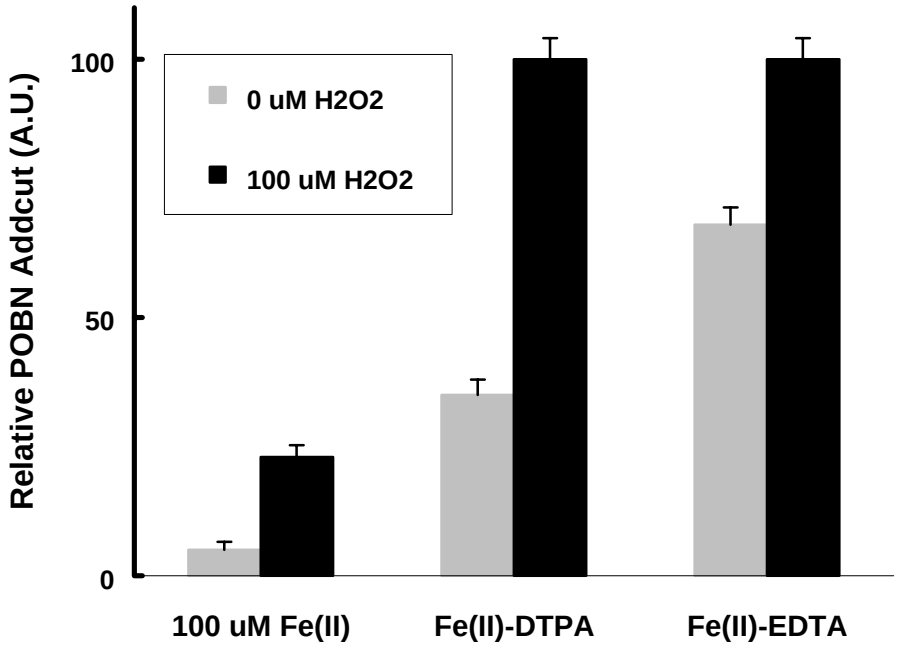

Figure 23. Chelator effect on glucose oxidation. The ordinate represents the POBN adduct yield in arbitrary units. Using 3-CP as a concentration standard, 100 A.U., the POBN adduct yield from 100 μM Fe^{2+}-EDTA and 100 μM H_2O_2, is about 0.61 μM POBN adduct. Counting from the left: Bar 1 to Bar 6. The chelator effects on enhancement of iron-mediated glucose oxidation were 7-fold for DTPA (bar 3), 14-fold for EDTA (bar 5), and 5-fold for H_2O_2-free iron (bar 2) higher than control (bar 1, 100 μM Fe^{2+} mediated), respectively (n=3, $p < 0.001$).

POBN Spin Adducts are formed *via* Iron-Mediated Glyceraldehyde Oxidation

Glyceraldehyde oxidation is a special process that differs from either chemical oxidation or glucose oxidation. Glyceraldehyde will autoxidize under physiological conditions to form several intermediates including hydroxypyruvaldehyde, hydrogen peroxide, hydroxyl radical, and carbon radicals. Its oxidative mechanism is represented in Figure 24.

To identify the possible initiators of glyceraldehyde oxidation, we first examined how important is $^{\bullet}OH$ derived by the chemistry presented in the box of Figure 24. In phosphate-buffered aerobic solution, 100 mM glyceraldehyde incubated with 10 mM POBN gave the EPR spectrum shown in Figure 25. Based on the hyperfine splitting parameters, this spectrum results from two radical species. One is a typical carbon-centered radical with $a^N \approx 15.7$ G and $a^H \approx 2.7$ G. Another is the POBN artifact [45] that arises from the breakdown of POBN ($a^N \approx 14.6$ G, $a^H \approx 14.6$ G). The same EPR spectrum, but with higher adduct yield, was obtained from 100 mM glyceraldehyde solution incubated with 10 mM POBN and 100 μM H_2O_2. These results suggest that the chemistry presented in the box of Figure 24 is a player for glyceraldehyde radical oxidations.

To further examine the significance of the chemistry of Figure 24 in glyceraldehyde oxidation, 100 mM glyceraldehyde was incubated with 50 mM DMPO spin trap in aerobic phosphate-buffered solution. EPR spectrum shown in Figure 26-a is almost the same as the standard DMPO/$^{\bullet}OH$ spectrum (Figure 20-b), which has

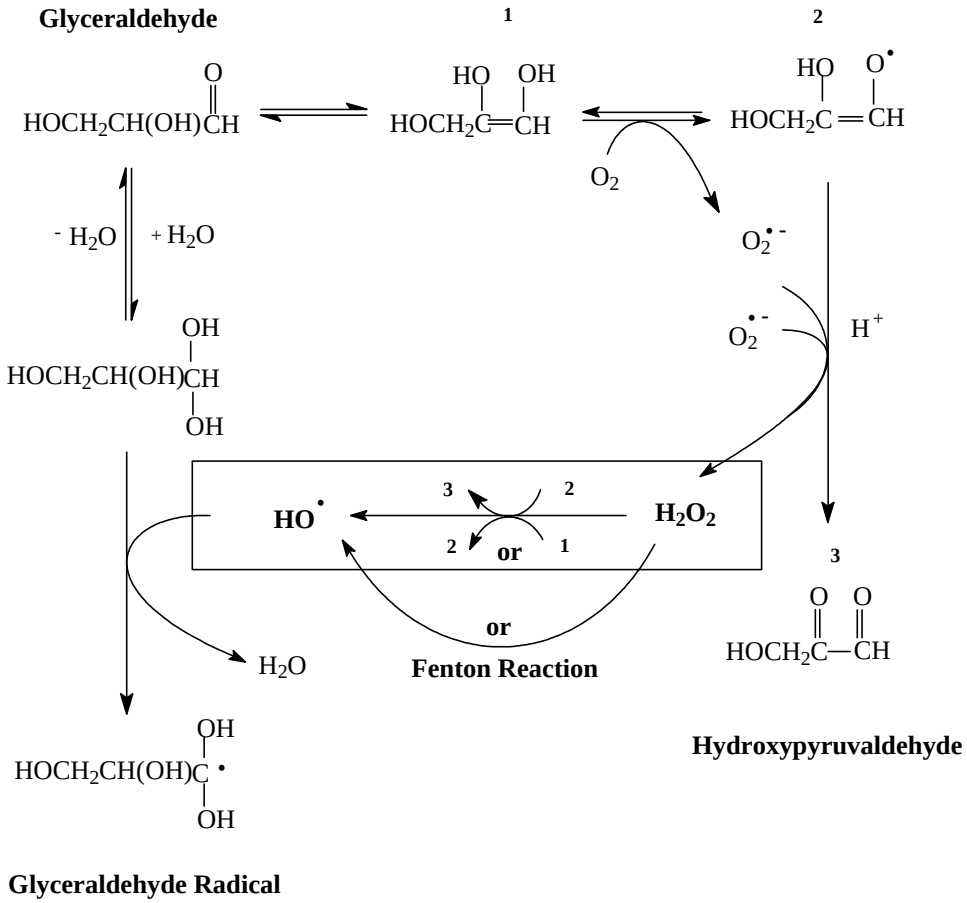

Figure 24. Scheme of glyceraldehyde oxidation [44].

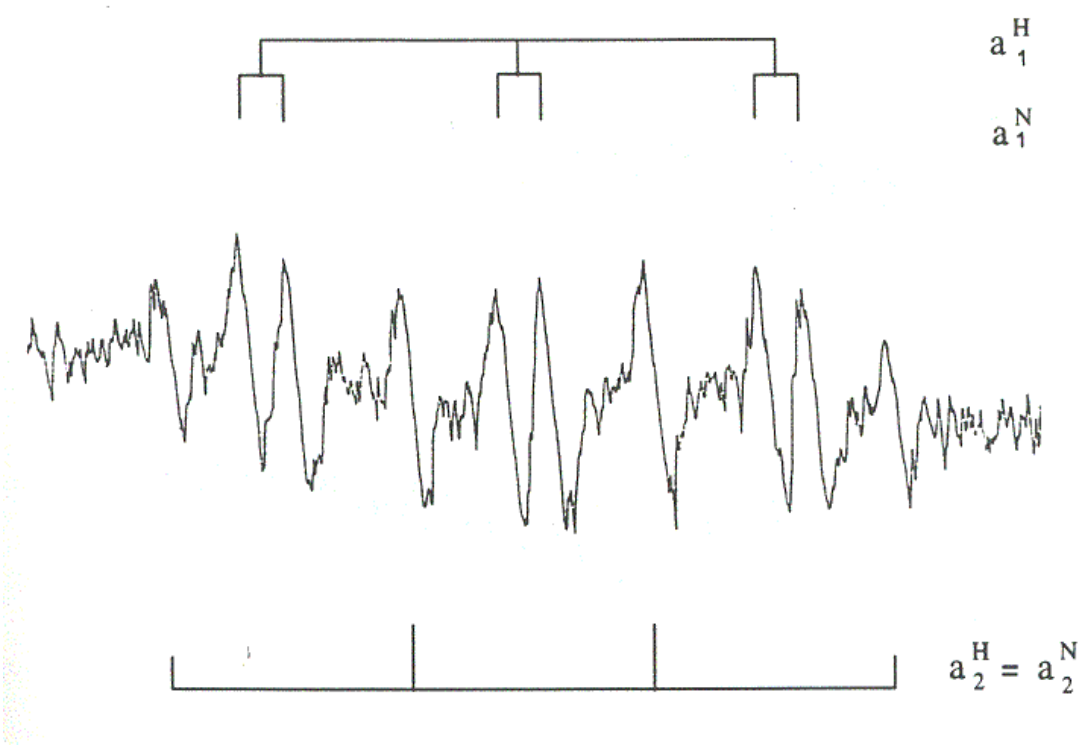

Figure 25. EPR spectrum of POBN adduct formed from glyceraldehyde (100 mM) oxidation. The POBN/$^{\bullet}$R represents a carbon-centered radical adduct with $a_1^N \approx 15.7$ G, $a_1^H \approx 2.7$ G. The POBN artifact has hyperfine parameters: $a_2^N \approx a_2^H \approx 14.6$ G).

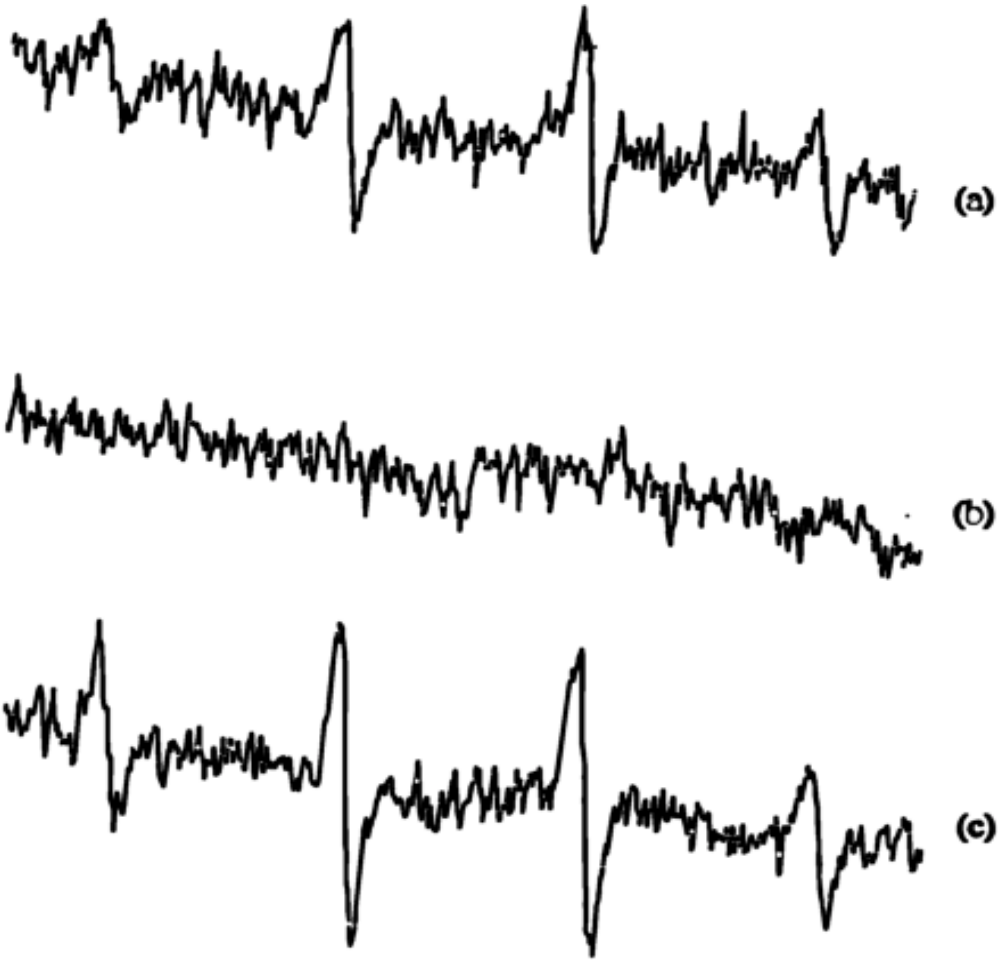

Figure 26. EPR spectrum of DMPO adduct formed from glyceraldehyde (iron free) oxidation.

(a) 100 mM glyceraldehyde incubated with 50 mM DMPO;
(b) added CAT (500 U/mL) into (a);
(c) added SOD (50 U/mL) into (a).

parameters $a^N \approx a^H \approx 14.9$ G. CAT as well as SOD was used to clarify that $^{\bullet}OH$ rather than alkoxyl radical being responsible for this spectrum. CAT totally inhibited DMPO adduct (see Figure 26-b); while SOD stimulated DMPO adduct formation, Figure 26-c. This result suggests that DMPO/$^{\bullet}OH$ rather than DMPO/alkoxyl radical was detected by EPR and that H_2O_2 was an intermediate.

Fe^{2+} as well as Fe^{3+} was added into glyceraldehyde-DMPO incubated solution to examine the role of iron in initiation of glyceraldehyde free radical oxidation. As shown in Figure 27-a, not only DMPO/$^{\bullet}OH$ adduct was detected by EPR, but also a carbon radical spin adduct DMPO/$^{\bullet}R$ ($a^N \approx 15.6$ G and $a^H \approx 22.4$ G) was detected when 100 μM Fe^{3+} was used to stimulate glyceraldehyde enolisation. These adducts, *i.e.* DMPO/$^{\bullet}OH$ and DMPO/$^{\bullet}R$, also resulted from 100 μM Fe^{2+}-glyceraldehyde incubations, but more DMPO/$^{\bullet}R$ adduct than DMPO/$^{\bullet}OH$ adduct was detected (see Figure 27-b). Furthermore, SOD stimulates formation of both spin adducts (see Figure 28-a); CAT completely inhibited DMPO/$^{\bullet}OH$ adduct formation, but failed to inhibited DMPO/$^{\bullet}R$ adduct formation (see Figure 28-b). These results suggest that the chemistries presented in Figure 24 are able to initiate glyceraldehyde radical oxidation, especially when iron is present. However, $^{\bullet}OH$ is not an essential reagent for initiating glyceraldehyde radical formation. Iron-oxygen complexes, rather than $^{\bullet}OH$ from pre-existing H_2O_2, are the most important initiators of glyceraldehyde radical oxidation.

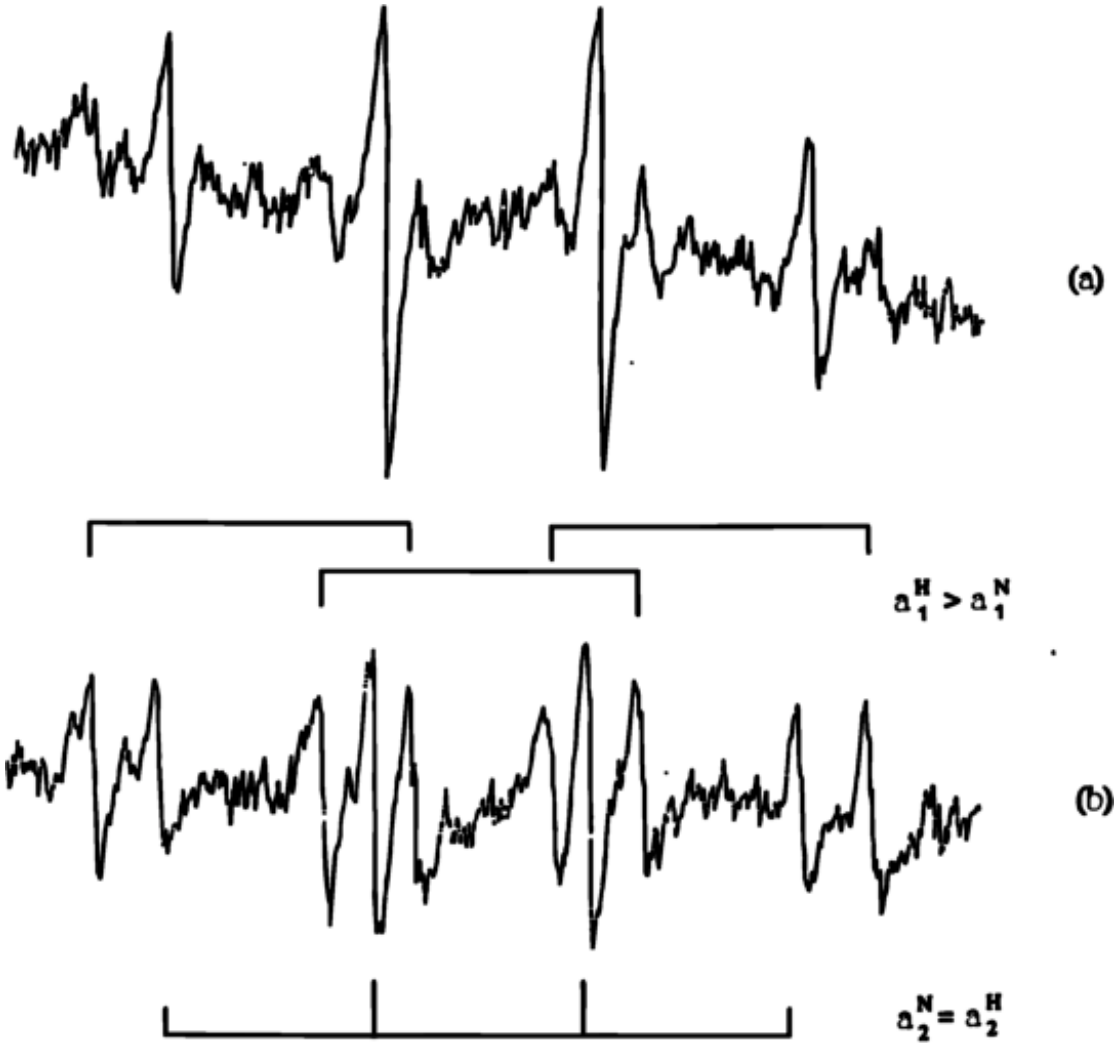

Figure 27. EPR spectrum of DMPO adduct formed from iron-mediated glyceraldehyde oxidation.

(a) 100 mM glyceraldehyde, 50 mM DMPO, and 100 μM Fe^{3+};

(b) 100 mM glyceraldehyde, 50 mM DMPO, and 100 μM Fe^{2+}.

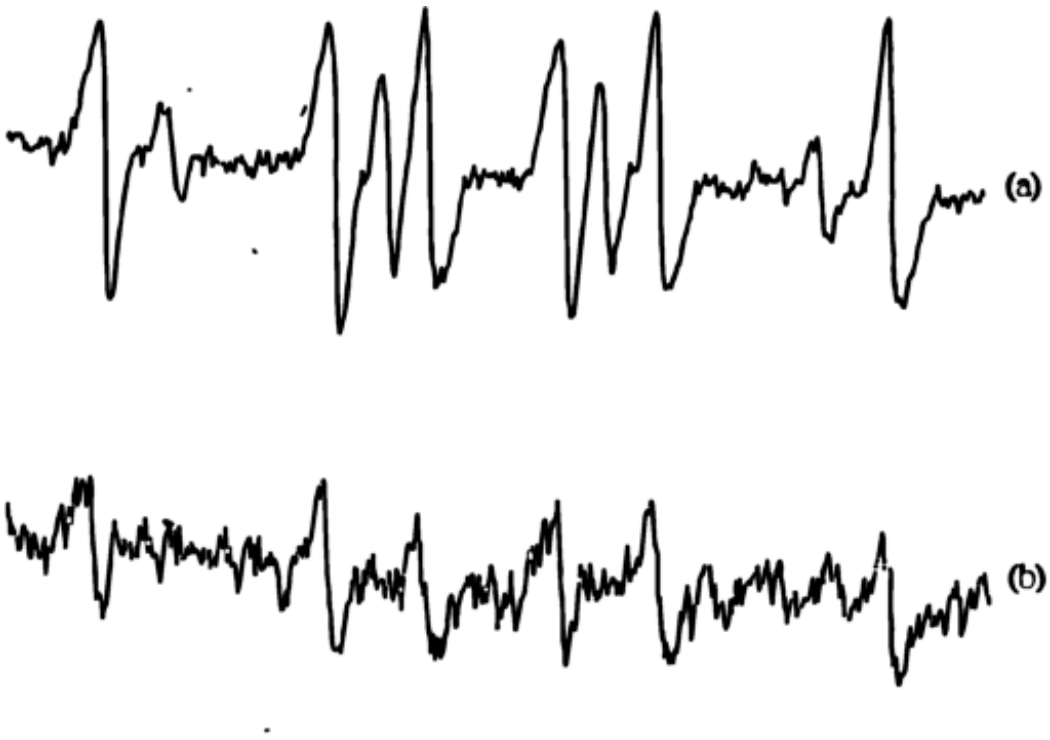

Figure 28. SOD and CAT effect on DMPO glyceraldehyde radical.

(a) added 50 U/mL SOD into 27-b;
(b) added 500 U/mL CAT into 27-b.

Fenton Efficiency Varies with $[O_2]/[H_2O_2]$ Ratio in Glyceraldehyde Oxidation

Unlike either chemical or glucose oxidation (Figures 11, 12, and 22), even at high $[Fe^{2+}]$ and low $[O_2]/[H_2O_2]$, the ordinate values of Figure 29 imply that the relative Fenton efficiency of glyceraldehyde oxidation is not high. This suggests that iron-oxygen complexes always dominate in glyceraldehyde radical formation and pre-existing H_2O_2 is unnecessary. Thus, Fe^{2+}-O_2 is the most important initiator of glyceraldehyde free radical-mediated oxidation. The $[O_2]/[H_2O_2]$ as well as the $[Fe^{2+}]$ dependence of Fenton efficiency is presented in Table 7.

Conclusions of Biochemical Oxidations

Unlike chemical free radical oxidation, many intermediates can be produced from biochemical material in the autoxidation process. It is possible that for the Fenton reaction could be involved in these processes even without preexisting H_2O_2. However, based on our observations, we suggest that $^{\bullet}OH$ formation from this Fenton route may contribute some macromolecule alterations, such as protein fragmentation, but it is a minor initiator for inducing biological target (glucose or glyceraldehyde) radical oxidations. Much like the role in chemical free radical oxidations, iron-oxygen complexes are most important initiators for formation of target radicals, especially in living systems where lower iron concentration, and higher $[O_2]/[H_2O_2]$ exist.

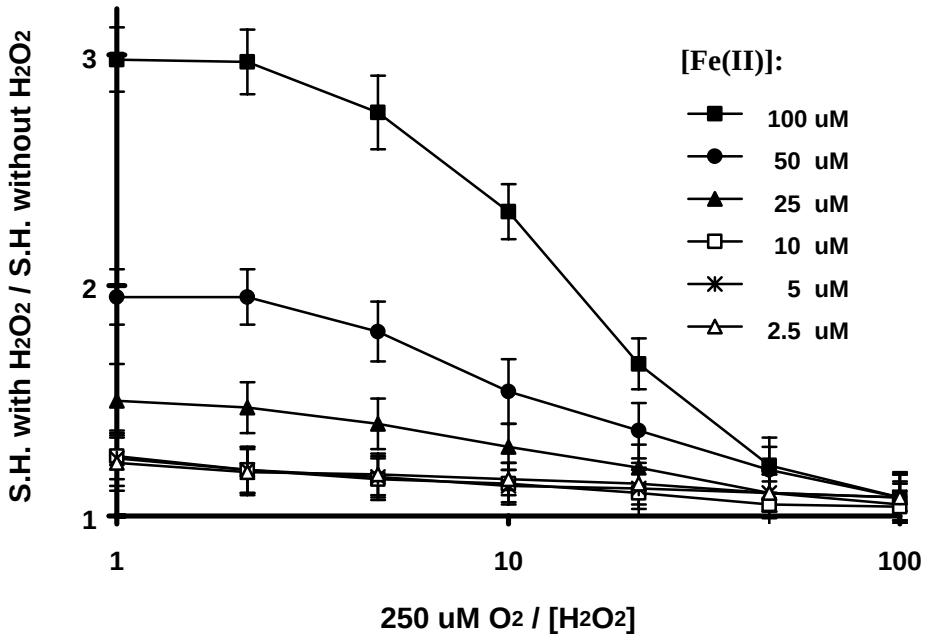

Figure 29. Relative Fenton efficiency of glyceraldehyde oxidation. 100 mM glyceraldehyde was incubated with 2.5, 5, 10, 25, 50, and 100 μM Fe^{2+}; with/without 2.5, 5, 10, 25, 50, 100, and 250 μM H_2O_2 under aerobic condition. All solutions were air-saturated, thus initial $[O_2] \approx 250$ μM. Values were expressed as means ± sd (n = 3).

Table 7. Fenton efficiency *vs*. Fe^{2+} as well as $[O_2]/[H_2O_2]$ in glyceraldehyde oxidation

Oxidizing System	High $[Fe^{2+}]$[a]	Low $[Fe^{2+}]$
High $[O_2]/[H_2O_2]$[b]	low[c]	low
Low $[O_2]/[H_2O_2]$	low (intermediate[e])	low

a: high $[Fe^{2+}] > 25$ μM; low $[Fe^{2+}] < 25$ μM.
b: high $[O_2]/[H_2O_2] \approx 10$ -100 ($[O_2] \approx 250$ μM in aerobic condition)
c: low Fenton efficiency means the ordinate in Figure 26 ≤ 2.
d: intermediate means ordinate in Figure 26 > 2. This occurs only with 100 μM Fe^{2+} and very low $[O_2]/[H_2O_2]$.

CHAPTER V

CELLULAR FREE RADICAL OXIDATIONS

Results and Discussion

Iron-mediated cellular lipid peroxidation is thought to be one of the key factors in cell injury. Polyunsaturated fatty acyl groups located in cell membranes are the principal targets for cellular lipid peroxidation. Polyunsaturated fatty acids (PUFA) usually contain methylene carbon bridges that have H atoms easily abstracted due to their low bond disassociation energy (Figure 3). Through bond rearrangements (reactions 1-3) as well as reaction 7, alkoxyl radical can be formed from the initiation and propagation steps of lipid peroxidation. Alkoxyl radical further undergoes β-scission (reactions 10-12) to form alkyl radicals, which can easily be detected by EPR spin trapping with POBN, and then to express the degree of cellular lipid peroxidation [46].

Theoretically, the favored positions attacked during lipid propagation radical are localized to the weakest point of lipid chain, *i.e*. the *bis*-allylic methylene positions (see Figure 3). The more *bis*-allylic methylene positions present in a lipid chain, the greater oxidizability of the lipid [47]. Thus, docosahexaenoic acid (DHA, 22:6n-3; Figure 30), a PUFA containing six double bonds with five methylene bridges, is especially susceptible to peroxidation.

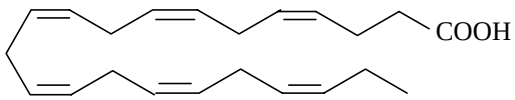

Figure 30. Structure of docosahexaenoic aid (DHA).

In our experiments, DHA was used to enrich fatty acid composition of L1210 murine leukemia cells. These lipid-modified cells were then used for studying the

initiation effects of cellular lipid peroxidations by the Fenton reaction as well as iron-oxygen complex reactions. The lipid-derived carbon-centered free radicals generated in L1210 cell oxidation were measured by EPR spin trapping with POBN. Our results suggests that cellular lipid peroxidation was predominately mediated by iron-oxygen complexes; the extracellular H_2O_2 might protect cellular lipid peroxidation by the Fenton reaction, and thereby inhibit the formation of iron-oxygen complexes due to $Fe^{2+} \rightarrow Fe^{3+}$.

Iron-Dependent Lipid-Derived Radical Formation *via* L1210 Lipid Peroxidation

After enrichment with DHA, L1210 cells were removed from the medium, washed in phosphate buffer, and immediately resuspended in phosphate buffer at a density of 5×10^6 cells/mL. This cell suspension was then incubated with POBN, ferrous iron, and/or H_2O_2.

As shown in Figure 31, lipid-derived radical formation illustrates an Fe^{2+}-dependent relationship when the enriched cells were incubated with 50 mM POBN and 0, 25, 50, 100 μM Fe^{2+}. Compared with POBN/single radical adduct EPR spectrum, for example Figure 6-a, we find that more than one POBN/carbon radical adduct is produced in L1210 lipid peroxidation. Based on the accepted lipid peroxidation mechanism and the EPR hyperfine splitting constants of these adducts, we assigned these adducts to two POBN alkyl radical adducts. One is the ethyl radical which probably derived from methyl terminus of DHA (a_1^N = 15.5 G, a_1^H = 2.9 G); the other probably is pentenyl

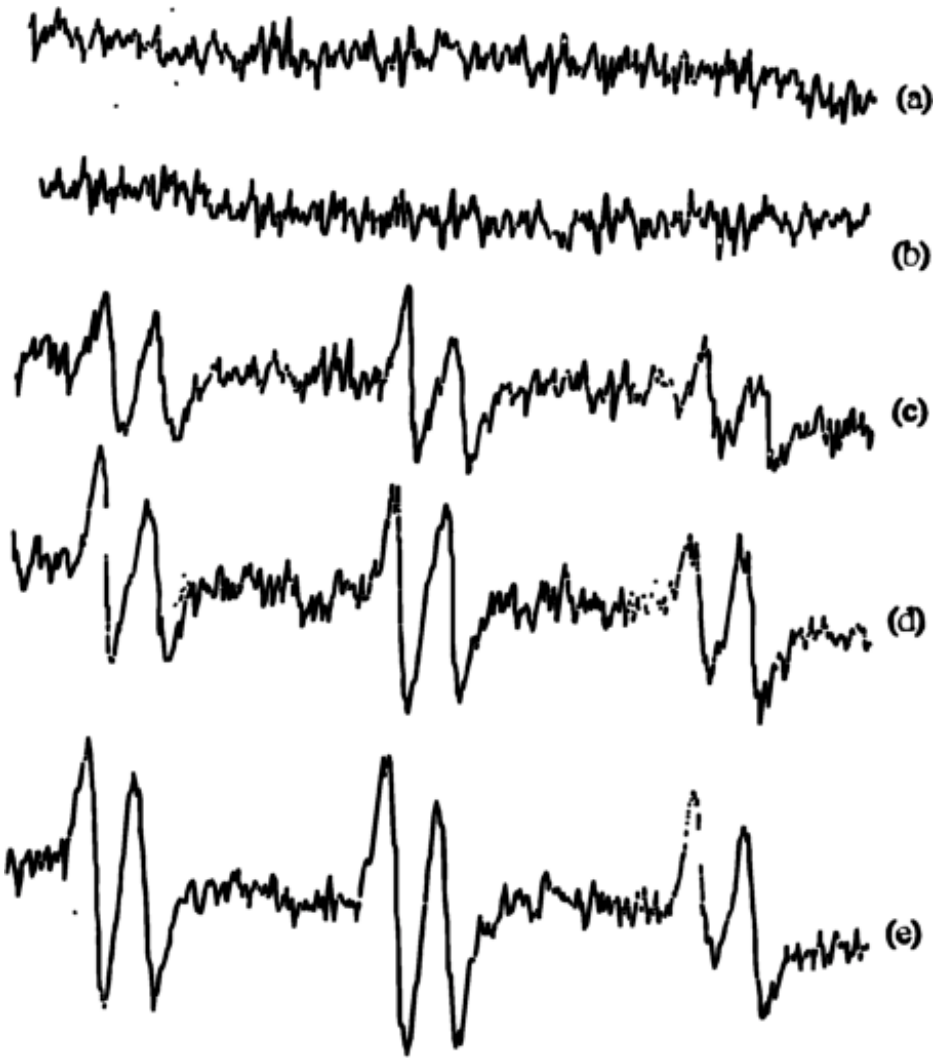

Figure 31. Fe^{2+}-dependent cellular lipid-derived radical formation. Five scans for EPR spectrum accumulation.

(a) Medium + 50 mM POBN + 100 μM Fe^{2+};
(b) DHA enriched L1210 cell + 50 mM POBN;
(c) DHA enriched L1210 cell + 50 mM POBN + 25 μM Fe^{2+};
(d) DHA enriched L1210 cell + 50 mM POBN + 50 μM Fe^{2+};
(e) DHA enriched L1210 cell + 50 mM POBN + 100 μM Fe^{2+}.

radical derived from pentenyl terminus of DHA (a_2^N = 15.8 G, a_2^H = 2.5 G).

However, to our surprise, the addition of H_2O_2 (25, 50, 100, and 250 μM) into 100 μM Fe^{2+}-mediated lipid peroxidation failed to stimulate POBN lipid-derived radical adducts. In fact the addition of H_2O_2 inhibits POBN adduct formation slightly. See Figure 32.

Conclusions of Cellular Lipid Peroxidation

Unlike the chemical oxidations and biochemical oxidations, cellular oxidation is a very complicated process. Extracellular Fe^{2+} has been reported to protect the intracellular space from H_2O_2 and thereby protect from the cell injury [48]. A similar proposal from our experiments is that extracellular H_2O_2 can protect the intracellular space from Fe^{2+} by initiating the Fenton reaction and thereby inhibiting the formation of iron-oxygen complexes. Thus, we suggest that cellular oxidation is predominately mediated by iron-oxygen complex reactions.

It has always been thought that it is very important to develop strategies to protect cells from $^{\bullet}OH$ radical formation arising from Fe^{2+} and pre-existing H_2O_2. For example, the removal of peroxides by cytoplasmic and mitochondrial glutathione peroxidase and peroxisomal catalase is very important [49]. However, based on our conclusions, the strategy of chelating iron should be given special attention due to the significance of iron's role in cellular lipid peroxidation.

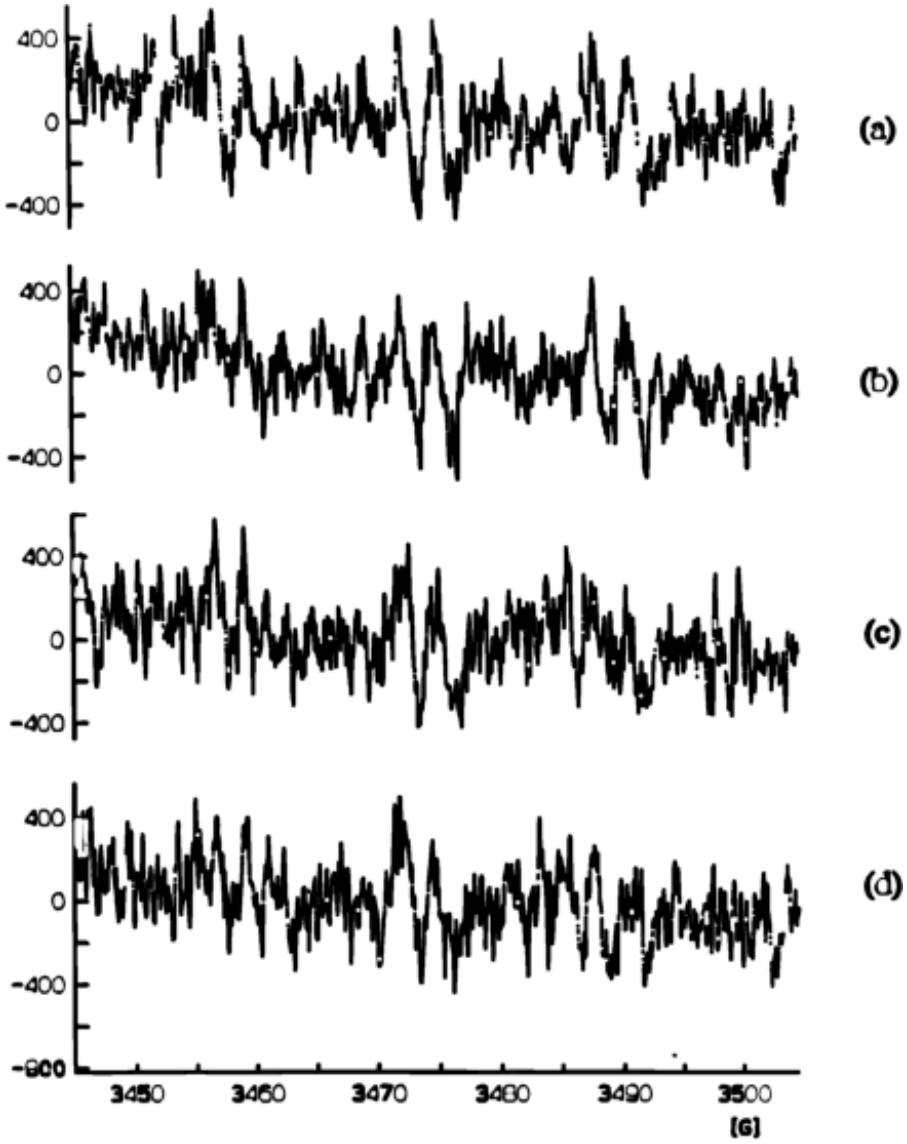

Figure 32. EPR spectrum of POBN cellular lipid radical adducts. Only one scan for EPR spectrum record.

(a) L1210 + 50 mM POBN + 0 μM H_2O_2 + 100 μM Fe^{2+};
(b) L1210 + 50 mM POBN + 25 μM H_2O_2 + 100 μM Fe^{2+};
(c) L1210 + 50 mM POBN + 50 μM H_2O_2 + 100 μM Fe^{2+};
(d) L1210 + 50 mM POBN + 100 μM H_2O_2 + 100 μM Fe^{2+}.

CHAPTER VI

PROSPECTS OF FUTURE RESEARCH

This study demonstrates that iron-oxygen complexes need to be considered as a primary initiator of chemical, biochemical, especially cellular free radical oxidation; however, most importantly, the exact identification of all lipid-derived radicals formed from lipid-modified cells has not been accomplished. Only an indirect interpretation for this has been reported [50]. This would seem to provide an impetus for our further research.

Based on lipid chemistry, there are several radicals produced during lipid peroxidation. The primary carbon-centered radicals are formed from fatty acid through H atom abstraction. The secondary radicals are lipid alkoxyl radicals and lipid peroxyl radicals from propagation reactions. The other kind of carbon-centered radicals are alkyl radicals which form from alkoxyl radicals undergoing β-scission. Thus, the suggested experiments to identify these radicals follow:

EPR/MNP Method

POBN spin trap was widely used in our study, but its hyperfine coupling constants alone are no enough to distinguish the differences in lipid-derived radicals. Thus, the MNP spin trap could be tried in these studies since it has different hyperfine coupling

constants for the different lipid-derived radicals. However, artifactual radical adducts will be formed from visible light exposure. The EPR triplet signal of this artifactual species usually overlaps the signal from the radical adducts of interest. Another disadvantage of MNP is its low water solubility. To overcome these weak points, we suggest an experimental scheme as shown in Figure 33.

EPR/POBN with HPLC as well as MS

Taking advantage of the unusual stability of carbon-centered radical adducts of POBN, HPLC and MS would be further used for isolation and identification. Although the EPR spectrum of lipid-derived radicals of POBN show the same or very similar hyperfine coupling constants, the EPR-HPLC analyses allow us to separate these adducts, and then the purified POBN adducts will be analyzed by MS. Furthermore, the authentic POBN radical adduct can be obtained from defined chemical systems, and used for further confirmation of these lipid-derived radicals. This experimental scheme is presented in Figure 34.

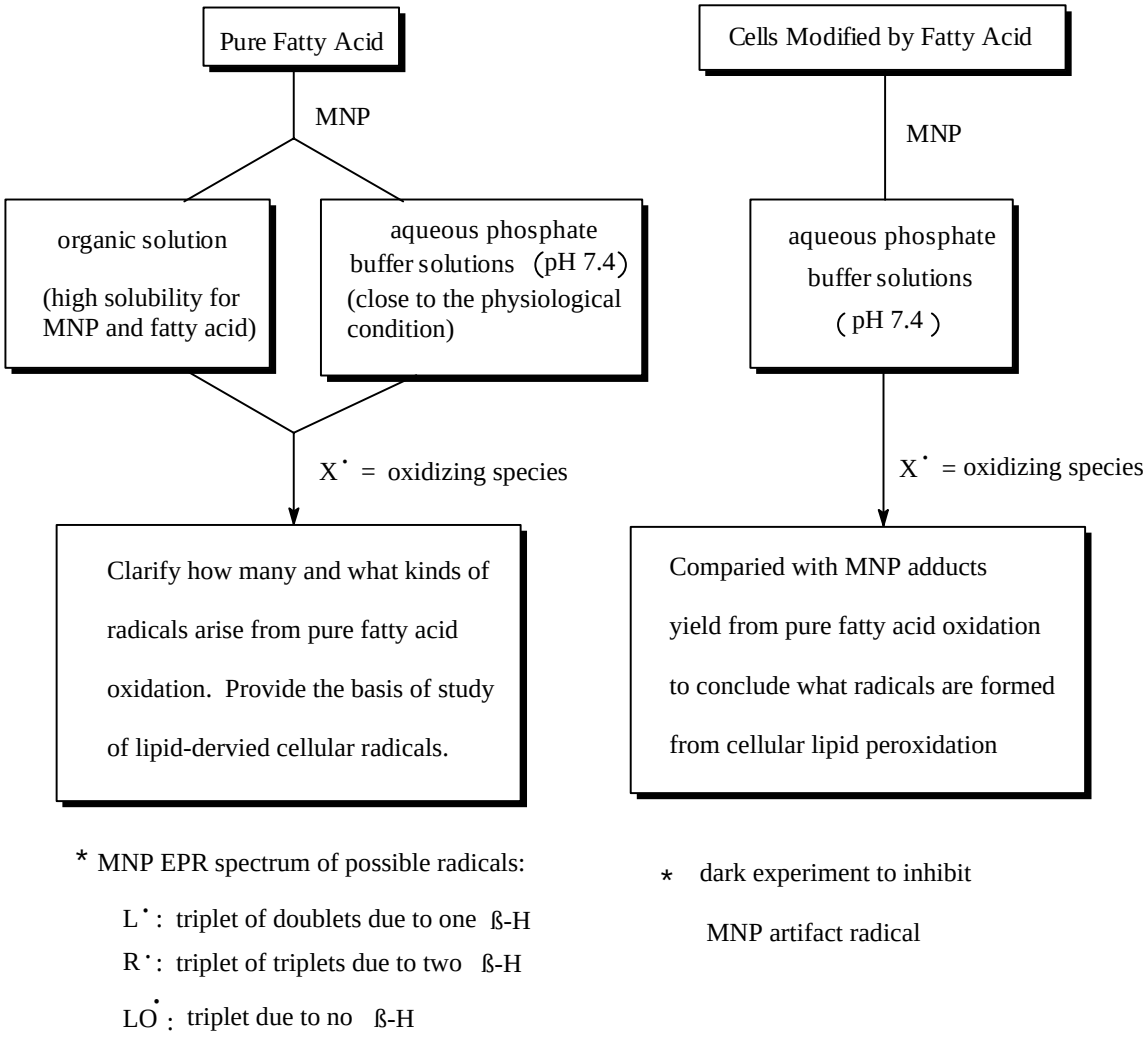

Figure 33. MNP Study of cellular lipid-derived radicals.

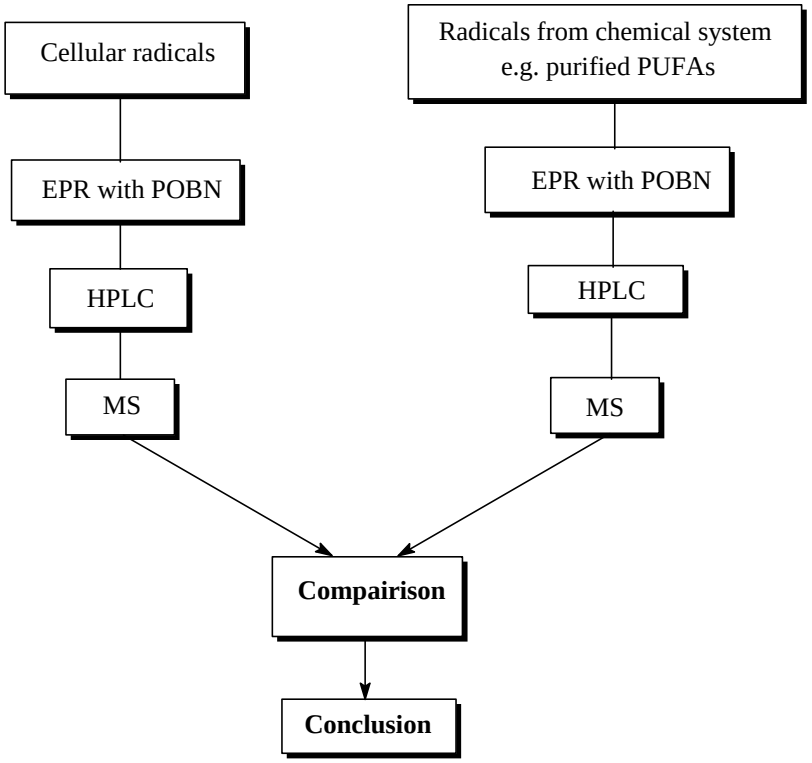

Figure 34. EPR/HPLC/MS method scheme.

REFERENCES

1. Rao PS, Cohen MV, Mueller HS: Production of free radicals and lipid peroxides in early experimental myocardial ischemia. *J. Mol. Cell. Cardiol*. **15**: 713-716, 1983.

2. Rowley B, Sweeney GD: Release of ferrous iron from ferritin by liver microsomes: a possible role in the toxicity of 2, 3, 7, 8-tetrachlorodibenzo-p-dioxin. *Can. J. Biochem. Cell Biol.* **62**: 1293-1300, 1984.

3. Keisari Y, Geva I, Macrophage oxidative burst (OB) and related cytotoxicity — II. Differential sensitivity of erythrocytes from various animals to OB dependent lysis. *Comp. Biochem. Physiol.* **80**: 163-166, 1985.

4. Kehrer JP: Free radicals as mediators of tissue injury and disease. *Critical reviews in toxicology*. **23**: 21-48, 1993.

5. Girotti AW: Mechanisms of lipid peroxidation. *Free Rad. Biol. Med*. **1**: 87-95, 1985.

6. Gardner HW: Oxygen radical chemistry of polyunsaturated fatty acids. *Free Rad. Biol. Med*. **7**: 65-86, 1989.

7. Marnett LJ, Wilcox AL. The chemistry of lipid alkoxyl radical and their role in metal-amplified lipid peroxidation. In: Rice-evens C, Halliwell B, Lunt GG, ed. *Free Radicals and Oxidative Stress: Environment, Drugs and Food Additives*. Biochem. Soc. Symp. **61**: 65-72, 1996.

8. Koppenol WH: Oxyradical reactions: from bond-dissociation energies to reduction potentials. *FEBS Letters*. **264**: 165-167, 1990.

9. Haber F, Weiss, JJ: The catalytic decomposition of hydrogen peroxide by iron salts. *Proc. Roy. Soc. London Ser.* A. **147**: 332-351, 1934.

10. McCord JM, Day ED: Superoxide-dependent production of hydroxyl radical catalyzed by iron-EDTA complex. *FEBS Letters*. **86**:139-142, 1978.

11. Goldstein S, Czapski G: The role and mechanism of metal irons and their complexes in enhancing damage in biological systems or in protection these systems from the toxicity of superoxide. *J. Free Rad. Biol. Med.* **2**: 3-11, 1986.

12. Fong KL, McCay PB, Poyer JL, Keele BB, Misra, H: Evidence that peroxidation of lysosomal membranes is initiated by hydroxyl free radicals produced during flavin enzyme activity. *J. Biol. Chem*. **248**: 7792-7797, 1973.

13. Lai CS, Piette LH: Hydroxyl radical production involved in lipid peroxidation of rat liver microsomes. *Biochem. Biophys. Res. Comm*. **78**: 51-59, 1977.

14. Lai CS; Piette LH: Spin-trapping studies of hydroxyl radical production involved in lipid peroxidation. *Arch. Biochem. Biophys*. **190**: 27-38, 1978.

15. Lai CS; Grover TA, Piette LH: Hydroxyl radical production in a purified NADPH — cytochrome c (P-450) reductase system. *Arch. Biochem. Biophys*. **193**: 373-378, 1979.

16. Girotti AW, Thomas JP: Superoxide and hydrogen peroxide-dependent lipid peroxidation in intact and Triton-dispersed erythrocyte membranes. *Biochem. Biophys. Res. Comm*. 118: 474-480, 1984.

17. Girotti AW, Thomas JP: Damaging effects of oxygen radical on resealed erythrocyte ghosts. *J. Biol. Chem*. **259**: 1744-1752, 1984.

18. Gutteridge JM: Reactivity of hydroxyl and hydroxyl-like radicals discriminated by release of thiobarbituric acid-reactive material from deoxyl sugars, nucleosides and benzoate. *Biochem. J*. **224**: 761-767, 1984.

19. Rush JD, Koppenol WH: Oxidizing intermediates in the reaction of ferrous EDTA with hydrogen peroxide. *J. Biol. Chem*. 261: 6730-6733, 1986.

20. Sutton HC, Vile GF, Winterbourn CC: Radical driven Fenton reaction — evidence from paraquat radical studies for production of tetravalent iron in the presence and absence of ethylenediaminetetraacetic acid. *Arch. Biochem. Biophys*. **256**: 462-471, 1987.

21. Hochstein P, Nordenbrand K, Ernster L: Evidence for the involvement of iron in the ADP-activated peroxidation of lipids in microsomes and mitochondria. *Biochem. Biophys. Res. Comm.* **14**: 323-328, 1964.

22. Svingen BA, O'Neal FO, Aust SD: The role of superoxide and singlet oxygen in lipid peroxidation. *Photochem. Photobiol*. **28**: 803-809, 1978.

23. Cabelli DE, Bielski HJ: Use of polyaminocarboxylates as metal chelators. In: Packer L, Glazer AN. ed. *Methods in Enzymology*. Academic Press. **186**: 116-120, 1990.

24. Fee JA, Valentine JS: Chemical and physical properties of superoxide. In: Michelson JM, McCord JM, Fridovich I. ed. *Superoxide and Superoxide Dismutases*. Academic Press, New York, 19-26. 1977.

25. Giulivi C, Hochstein P, Davies KJ: Hydrogen peroxide production by red blood cells. *Free Rad Biol Med*. **16**: 123-129, 1994.

26. Jones DP: Intracellular diffusion gradients of O_2 and ATP. *Am. Physol. Soc*. 1986. C663-675.

27. Aust SD, Svingen BA: The role of iron in enzymatic lipid peroxidation. In: Pryor WA. ed. *Free Radicals in Biology*. Vol:V, Academic Press, New York. 1982.

28. Tien M, Svingen BA, Aust SD: Superoxide dependent lipid peroxidation. *Fed. Proc*. **40**: 179-182, 1981.

29. Morehouse LA, Tien M, Bucher JR, Aust SD: Effect of hydrogen peroxide on the initiation of microsomal lipid peroxidation. *Biochem. Pharmacol.* **32**: 123-127, 1983.

30. Walling C: Fenton's reaction revisited. *Accts. Chem. Res.*. **8**: 125-131, 1975.

31. Koppenol WH, Liebman JF: The oxidizing nature of hydroxyl radical — A comparison with the ferryl ion. *J. Phys. Chem.* **88**: 99-105, 1984.

32. Ponka P: Physiology and pathophysiology of iron metabolism: implications for iron chelation therapy in iron overload. In: Bergeron RJ, Britterham GM. ed. *The Development of Iron Chelators for Clinical Use*. CRC Press. 1994, 1-32.

33. Harris DC, Aisen P: Facilitation of Fe(II) autoxidation by Fe(III) complexing agents. *Biochim. Biophys. Acta.* **329**:156-158, 1973.

34. Lind MD, Hoard JL, Hamor MJ, Hamor TA, Hoard JL: Sterochemistry of ethylenediaminetetraacetato complexes. *Inorg. Chem*. **3**:34-43. 1964.

35. Buettner GR: Use of ascorbate as test for catalytic metals in simple buffers. In: Packer L, Glazer AN. ed. *Methods in Enzymology*. Academic Press. **186**: 125-127, 1990.

36. Janzen EG: Spin trapping. *Acc. Chem. Res*. **4**: 31-40. 1971

37. Janzen EG: A critical review of spin trapping in biological systems. In: Pryor WA. ed. *Free Radical in Biology.* Vol: IV. Academic Press. New York. 115-153, 1980.

38. Buettner GR: Spin trapping: ESR parameters of spin adducts. *Free Rad. Biol. Med*. **3**: 259-303, 1987.

39. Janzen EG, Wang YY, Shetty RV: Spin trapping with α-pyridyl 1-oxide *N-tert*-butyl nitrones in aqueous solutions. *J. Am. Chem. Soc*. **100**: 2923-2925, 1978.

40. Stadtman ER, Berlett BS: Fenton chemistry. Amino acid oxidation. *J. Biol. Chem.* **266**: 17201-17211, 1986.

41. Buettner GR, Doherty TP, Patterson LK: The kinetics of the reaction of superoxide radical with Fe^{3+} complexes of EDTA, DTPA and HEDTA. *FEBS Letters* **158**: 143-146, 1983.

42. Zang V, Van Eldik, R: Kinetics and mechanism of the autoxidation of iron(II) induced through chelation by ethylenediaminetetraacetate and related ligands. *Inorg. Chem.* **29**: 1705-1711, 1990.

43. Wolff SP, Bascal Z, Hunt JV: Autoxidative glycosylation: free radicals and glycation theory. In: Kunio Yagi, ed. *The Maillard Reaction in Ageing, Diabetes and Nutrition*. Alan R. Liss, Inc. 247-275, 1989.

44. Thornalley P, Wolff S, Crabbe J, Stern A: The autoxidation of glyceraldehyde and other simple monosaccharides under physiological conditions catalysed by buffer ions. *Biochim. Biophys. Acta*. **797**: 276-287, 1984.

45. Britigan BE, Pou S, Rosen GM, Lilleg DM, Buettner GR: Hydroxyl radical is not a product of the reaction of xanthine oxidase and xanthine. *J. Biol. Chem.* **263**: 17533-17538, 1990.

46. North JA, Spector AA, Buettner GR: Detection of lipid radicals by electron paramagnetic resonance spin trapping using intact cells enriched with polyunsaturated fatty acid. *J. Biol. Chem.* **267**: 5743-5746, 1992.

47. Wagner BA, Buettner GR, Burns CP. Free radical-mediated lipid peroxidation in cells: oxidizability is a function of cell lipid *bis*-allylic hydrogen content. *Biochemistry*. **33**: 4449-4453, 1994.

48. Hempel SL, Buettner GR, Wessels DA, Galvan GM, O'Malley YQ: Extracellular iron(II) can protect cells from hydrogen peroxide. *Arch Biochem. Biophys.* **330**: 401-408, 1996.

49. Thomas JP, Maiorino M, Ursini F, Girotti AW: Protective action of phospholipid hydroperoxide glutathione peroxidase against membrane-damaging lipid peroxidation. In *stiu* reduction of phospholipid and cholesterol hydroperoxides. *J. Biol. Chem*. **265**: 454-461, 1990.

50. North JA, Spector AA, Buettner GR: Cell fatty acid composition affects free radical formation during lipid peroxidation. *Am. J. Physiol.* **267** *(Cell Physiol. 36):* C117-C188, 1994.